inhibitor of the Wnt/β-catenin pathway [13]. In the Wnt/β-catenin pathway, axin, a component of the destruction complex that regulates β-catenin, is degraded by poly(ADP-ribosyl)ation catalyzed by tankyrase 1 and its isoform, tankyrase 2. So far, there has been no other report of screening for tankyrase 1 inhibitors, probably due to the difficulty of efficiently preparing active tankyrase 1. Here, we describe an efficient system for screening tankyrase 1 inhibitors, amenable to a high-throughput method, using fission yeast strain overexpressing human tankyrase 1 (TNKS1). A yeast cell-based phenotypic drug screening system has advantages over in vitro assay system, because cell-permeability and toxicity of chemical compounds can be simultaneously tested during screening. Schizosaccharomyces pombe is an excellent model system: genetic manipulation is easy; it is cost-effective; and the cells grow rapidly, making possible rapid and high-throughput drug screening. Moreover, S. pombe has no poly(ADP-ribose) polymerase homolog. Thus, this yeast can be used as a "living test tube" to detect the enzymatic activity of the ectopically expressed PARPs. Taking advantage of this approach, we identified flavone as a tankyrase 1 inhibitor.

2. Materials and methods

2.1. Reagents

Tested compounds were supplied from the RIKEN Natural Products Depository (NPDepo). WST-1 and 1-methoxy-PMS were obtained from Dojindo, and both reagents were solubilized in 20 mM Hepes (pH 7.4). These compounds were added to the yeast culture at final concentrations of 0.25 mM for WST-1 and 0.01 mM for 1-methoxy-PMS. Flavone, 3-aminobenzamide (3AB), a mouse monoclonal anti-tubulin antibody (B5-1-2), and a mouse monoclonal anti-FLAG antibody (M2) were purchased from Sigma. Mouse monoclonal anti-PAR antibody (clone 10HA) was purchased from Trevigen, and rabbit polyclonal anti-tankyrase (H-350) antibody was purchased from Santa Cruz Biotechnology. The horseradish peroxidase (HRP)-linked anti-mouse IgG and anti-rabbit IgG and the FITC-conjugated anti-mouse IgG were obtained from GE Healthcare. The VECTASHIELD Mounting Medium was purchased from Vector Lab.

2.2. Introduction of the human TNKS1 into the fission yeast cells

The human TNKS1 gene was cloned as Gateway entry clones by recombining the PCR-amplified open reading frame (ORF) of human cDNAs as reported [14]. The TNKS1 entry clones were produced as an N-type clone, with an intrinsic STOP codon at the end of the ORF, and as an F-type clone with no STOP codon, for producing a C-terminal tagged protein. Sequence analysis revealed that the PCR-amplified TNKS1 gene contained three nucleotide mutations (C248A, A3002G, and G3098A). The PARP-dead mutant TNKS1 carrying a single amino acid change (H1184A) was constructed as follows: the point mutation in the PARP domain was obtained by PCR amplification of the Gateway entry plasmid containing TNKS1 using the primers tank1_H1184A_Fwd 5′-GAGCGCATGTTGTTTGCTGGTTCTCCTTTCATTAATG-3′ and tank1_H1184A_Rev 5′-CATTAATGAAAGGAGAACCAGCAAACAACATGCGCTC-3′. Both types of the wild-type (WT) and mutant TNKS1 genes were transferred to the fission yeast expression vector pDUAL-FFH1c by recombination, in order to produce the native-type TNKS1 protein (N-type) or the C-terminally FLAG–FLAG–His6-tagged TNKS1 protein (F-type), respectively, under the control of the thiamine-regulatable nmt1 promoter [15,16]. Yeast genetic manipulation was performed as described [17]. In order to elevate the drug sensitivity of the fission yeast strains, we deleted the pmd1 and bfr1 genes, which encode ABC transporters responsible for an efflux of various antibiotics [18,19]. The

pmd1::ura4 fragment [18] was PCR-amplified using primers that flanked the pmd1 gene (SN6F1, 5′-TTCGTTTTATCAATTCCATT-3′; SN6R1, 5′-AATAAAACACAAACCTGACT-3′) [20] and was inserted into the pmd1 locus of strain JY878 (h⁹⁰ ade6-M216 leu1-32 ura4-D18), producing the strain YY278 (h⁹⁰ ade6-M216 leu1-32 ura4-D18 pmd1::ura4). YY278 was crossed with YY269 (h⁻ ade6-M210 leu1-32 ura4-D18 bfr1::ura4), which was constructed in Ref. [19]. The resultant diploid cells were sporulated and subjected to dissection. One of the progeny, YY299 (h⁹⁰ ade6-M216 leu1-32 ura4-D18 pmd1::ura4 bfr1::ura4), was chosen for use as the drug-sensitive host strain. The gene disruption was verified by uracil prototrophy and PCR. To produce the TNKS1 overexpression strains, we introduced the N-type and F-type TNKS1 genes, with or without catalytic mutations, into the leu1 locus of YY299. Although the PCR-amplified TNKS1 gene contains three nucleotide mutations (C248A, A3002G, and G3098A), resulting in amino acid alterations (Pro83Gln, Glu1001Gly, and Met1266Ile), we concluded that these changes cause no adverse effect on the enzyme activity of tankyrase 1, since overexpression of TNKS1 showed sufficient enzyme activity in yeast (see below).

2.3. High-throughput drug screening using a WST-1 reagent

We used WST-1 to quantify yeast cell growth based on mitochondrial dehydrogenase activity, which cleaves the tetrazolium salt WST-1 to produce the formazan dye. Fission yeast cells pregrown on synthetic dextrose (SD) solid medium at 30 °C for 2–3 days were subsequently grown for 24 h with vigorous shaking in minimal medium (MM) containing 10% (v/v) of SD liquid media, in order to supply a small amount of thiamine. This pre-culture was then 200-fold diluted in MM media and grown at 30 °C for 18 h. Finally, the prepared WST-1 mixture was added to the yeast culture, and absorbance of the formazan product was measured after incubation for more than 3 h (absorption wavelength, 450 nm; reference wavelength, 650 nm). For the primary high-throughput drug screening, yeast cells were cultured in 20 μL of MM media containing chemical compounds from the NPDepo library at concentrations of 10, 5, 2.5, and 1.25 μg/mL using 384-well plates (see Supplementary Fig. 1); all cultures were dispensed using a Biomek NX automation instrument. The WST-1 mixture was added to the yeast culture using a Biotec mini-Gene LD-01 single-line dispenser device. Thorough vortexing of the 384-well microplates was performed using a Biotec Bio-mixer. We selected the compounds whose Z scores of absorbance calculated every 88 chemical compounds were over 10 as hits. For the secondary assay, yeast cells were cultured in 50 μL of MM media with varying concentrations of flavone or 3AB using 96-well plates, and WST-1 mixture was added to the culture.

2.4. Immunoblotting

Cells grown in MM media with or without drugs were harvested after 18–22 h. Lysates were prepared as described [21] and analyzed by SDS–PAGE and Western blotting using the anti-PAR antibody (1:1000), the anti-tankyrase antibody (1:1000), the anti-tubulin antibody (1:5000), the HRP-linked anti-mouse antibody (1:10,000), or the HRP-linked anti-rabbit antibody (1:10,000).

2.5. Immunofluorescence staining

Indirect immunofluorescence staining was performed as described [22]. Briefly, HeLa I.2.11 cells were transfected with pLPC/FN-tankyrase-1 vector [3] using a standard electroporation method. After incubation for 18–21 h with test compounds at 37 °C, cells were fixed with 2% paraformaldehyde/phosphate-buffered saline (PBS) and permeabilized with 0.5% Nonidet P-40/PBS. Cells

were blocked in PBS containing 1% bovine serum albumin, and incubated with mouse anti-FLAG antibody (2 μg/mL). Next, the cells were washed and further incubated with FITC-conjugated sheep anti-mouse immunoglobulin (1:25). Cellular DNA was stained with 4,6-diamino-2-phenylindole (DAPI) using the VECTA-SHIELD Mounting Medium. Images were collected using an Olympus IX-71 microscope with a DP70 digital camera.

3. Results

3.1. Construction of fission yeast strains that overexpress human tankyrase 1

To test the effects of TNKS1 gene overexpression on the cell growth of S. pombe, we introduced PCR-amplified human TNKS1 genes into a drug-sensitive strain lacking both pmd1 and bfr1 [18,19]. The native form of the TNKS1 gene, containing the intrinsic termination codon (N-type), and the C-terminally FLAG/His6-tagged form (F-type) were integrated into the leu1 locus. The genes were under control of the thiamine-regulatable nmt1 promoter: expressed on MM media lacking thiamine, but repressed on SD media containing thiamine. Expression of both the N-type and F-type TNKS1 genes caused growth retardation in fission yeast cells on MM, but not under uninduced conditions on SD (Fig. 1A). Overexpression of the F-type TNKS1 gene caused a more severe growth defect than that of N-type, because of the higher enzymatic activity of the F-type tankyrase 1 protein (see below, Fig. 1B). It seems possible that C-terminal tagging has some role in supporting correct folding in the fission yeast cells. In contrast to the growth defect of the WT TNKS1 overexpression strains, overexpression of the PARP-dead mutant (H1184A) failed to induce growth arrest (Fig. 1A). Furthermore, immunoblotting analysis with the anti-PAR antibody showed that poly(ADP-ribosyl)ation of proteins oc-

curred in S. pombe cells overexpressing WT TNKS1 (both N-type and F-type), but not in those overexpressing the catalytically dead TNKS1 (Fig. 1B). In mammalian cells, known targets of tankyrase 1 are TRF1 and axin, neither of which are conserved in fission yeast [5,13]. Since tankyrase 1 is auto-poly(ADP-ribosyl)ated, the major poly(ADP-ribosyl)ated protein with a molecular mass of around 140 kDa could be the tankyrase 1 protein itself overexpressed in fission yeast (see Fig. 1B, lane 3). Other poly(ADP-ribosyl)ated proteins were not identified in this study. The levels of protein poly(ADP-ribosyl)ation were correlated with inhibitory effects on cell growth, suggesting that the tankyrase 1 enzymatic activity is responsible for the growth defect caused by TNKS1 overexpression. This growth retardation phenotype can be used for detecting inhibitory activity against tankyrase 1, because inhibition should alleviate the growth phenotype.

3.2. Screening for compounds that rescue the TNKS1-induced growth arrest

We developed a liquid assay method for drug screening in a high-throughput manner, using the strain that overexpresses the N-type TNKS1 gene (see Section 2; Supplementary Fig. 1). We carried out high-throughput screening of ~7000 purified chemicals from the RIKEN NPDepo library, searching for compounds that rescue cell growth. We monitored cell growth using a WST-1 colorimetric assay. Flavone was identified as a compound that alleviates the yeast growth retardation (Supplementary Figs. 1 and 2A). The effective concentration of flavone was ~10 μM, much lower than that of the pan-PARP inhibitor 3AB (~10 mM) (Fig. 2B). We next examined whether flavone and 3AB decreased the PAR level of proteins, using yeast whole-cell lysates prepared from cells overexpressing the F-type TNKS1 gene; poly(ADP-ribosyl)ation was more evident in these cells than in cells overexpressing the
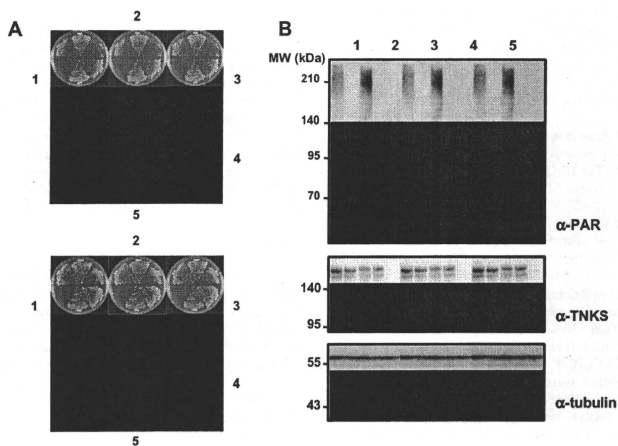
Fig. 1. Overexpression of the human tankyrase 1 gene caused growth defect and poly(ADP-ribosyl)ation in fission yeast. (A) Growth defect of the TNKS1 overexpression strains. The fission yeast cells harboring the N-type or F-type TNKS1 (WT or mutant H1184A) were streaked on MM (for overexpression; upper panel) and SD (for repression; lower panel) and incubated at 30 °C for 3 days. 1: N-type WT TNKS1; 2: N-type inactive mutant TNKS1; 3: F-type WT TNKS1; 4: F-type inactive mutant TNKS1; and 5: empty control. (B) Western blot analysis of yeast whole-cell lysates. Cells were grown in MM media for 22 h and harvested to prepare lysates. The lysates were subjected to Western blot analysis with anti-PAR, anti-tankyrase, and anti-tubulin antibodies.
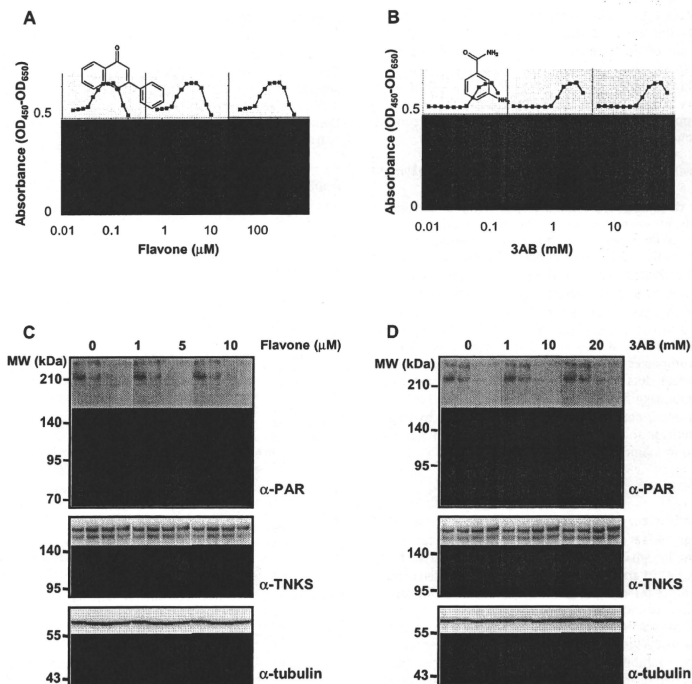
A

B

C

D

Fig. 2. Effects of flavone and a pan-PARP inhibitor 3AB on the growth of TNKS1 overexpression cells and poly(ADP-ribosyl)ation of yeast proteins. (A and B) Cells overexpressing the N-type TNKS1 were treated with various concentrations of flavone (A) and 3AB (B). After an 18-h incubation of 50 μL of cell culture with various concentrations of drugs as indicated, we assessed cell growth using WST-1. (C and D) Effects of flavone and 3AB on poly(ADP-ribosyl)ation were analyzed by detecting PAR levels of proteins, using yeast cell lysates. Cells overexpressing the F-type TNKS1 were grown in MM media containing flavone (C) or 3AB (D) at various concentrations as indicated for 18 h, then harvested and analyzed with Western blotting.
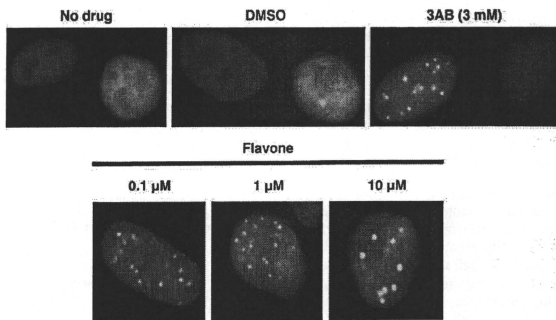

Fig. 3. Assembly of tankyrase 1 at the telomere regions by flavone in mammalian cells. Cells transfected with FN-tankyrase 1 construct were treated with flavone, 3AB, and DMSO at concentrations as indicated. Tankyrase 1 was detected using indirect immunofluorescence staining with the anti-FLAG antibody (shown in green). DNA was detected by staining with DAPI (shown in blue). (For interpretation of the references to color in this figure legend, the reader is referred to the web version of this article.)

N-type TNKS1 (see Fig. 1B). In agreement with effects on the cell growth, both flavone and 3AB almost completely inhibited poly-(ADP-ribosyl)ation of yeast proteins at concentrations of 5 μM and 10 mM, respectively (Fig. 2C and D). It has previously been reported that flavone inhibits PARP1 [23]. We also confirmed flavone's inhibitory activity against PARP1 by ELISA (Supplementary method and Supplementary Fig. 2). However, much higher concentrations of flavone were required to inhibit PARP1 activity.

3.3. Treatment with flavone causes punctate localization of tankyrase 1

To evaluate the tankyrase 1-inhibitory activity of flavone in mammalian cells, we examined the effect of flavone on the subcellular localization of tankyrase 1, using transient overexpression of TNKS1 in mammalian cells and indirect immunofluorescence staining [22]. This assay is based on the principle that TRF1 dissociates from telomeres in cells overexpressing tankyrase 1. When the TNKS1 gene was overexpressed in the nucleus, tankyrase 1 is flatly distributed in the nucleoplasm (Ref. [22] and Fig. 3). However, inhibition of tankyrase 1 by 3AB (3 mM) stabilizes the tankyrase 1–TRF1 complexes on telomeres, which can be visualized as punctate nuclear dots of exogenous tankyrase 1. Upon treatment with flavone, significant punctate staining of the tankyrase 1 foci appeared under concentrations ranging from 0.1 to 10 μM. These results indicate that flavone inhibits tankyrase 1 not only in yeast but also in mammalian cells.

4. Discussion

The PARP family of enzymes has attracted attention as targets of therapeutic drugs, and several assay systems have been established. Indeed, screening for small-molecule inhibitors against two PARP family members, PARP1 and PARP2, was previously reported in budding yeast [24]. Since tankyrase 1 is a therapeutic target for cancer therapy, especially for BRCA-associated cancers, it was important to develop of a facile screening method applicable to high-throughput assay. In this study, we established a phenotypic screening system for tankyrase 1 inhibitors, using genetically engineered fission yeast strains, and demonstrated its usefulness by screening a chemical library and identifying flavone as a tankyrase 1 inhibitor. Although the tested compounds supplied from RIKEN NPDepo library contain several flavonoids, only flavone was identified as a hit compound in this screening, suggesting that flavone is more potent in inhibiting tankyrase 1 than other flavonoids in the library. Flavone was reported as an inhibitor of PARP1 by Geraets et al. [23]. In their in vitro assay, the activity of PARP1 was inhibited by 100 μM flavone; the inhibition was slightly stronger than the inhibition by 3AB at the same concentration [23]. These findings are consistent with our ELISA (Supplementary Fig. 2). Because the effective concentration of flavone for inhibiting tankyrase 1 activity (0.1–10 μM) (see Fig. 3) was much lower than for PARP1, flavone may preferentially inhibit tankyrase 1 rather than PARP1 in vivo.

When human tankyrase 1 was overexpressed in fission yeast having no intrinsic PARPs, poly(ADP-ribosyl)ation of yeast proteins was observed, although these proteins have yet to be unidentified. The conventional method for measuring tankyrase activity is still based on a radioactive format, whereas a non-radioactive ELISA method has been established for PARP1. It should be noted that in our method, drug effects on PAR activity of tankyrase are easily detectable by Western blot analysis using yeast cell lysates, and can be detected without use of a radioisotope-labeled substrate (NAD$^+$). Thus, a yeast cell-based drug screening using gene overexpression can overcome potential difficulties in establishing a high-throughput assay for tankyrases, and has great potential for identifying and developing inhibitors of tankyrases and other PARP family enzymes.

Appendix A. Supplementary data

Supplementary data associated with this article can be found, in the online version, at doi:10.1016/j.bbrc.2010.03.021.

References

[1] J. Amé, C. Spenlehauer, G. de Murcia, The PARP superfamily, Bioessays 26 (2004) 882–893.
[2] S. Smith, I. Giriat, A. Schmitt, et al., Tankyrase, a poly(ADP-ribose) polymerase at human telomeres, Science 282 (1998) 1484–1487.
[3] H. Seimiya, Y. Muramatsu, S. Smith, et al., Functional subdomain in the ankyrin domain of tankyrase 1 required for poly(ADP-ribosyl)ation of TRF1 and telomere elongation, Mol. Cell. Biol. 24 (2004) 1944–1955.
[4] B. van Steensel, T. de Lange, Control of telomere length by the human telomeric protein TRF1, Nature 385 (1997) 740–743.
[5] W. Chang, J.N. Dynek, S. Smith, TRF1 is degraded by ubiquitin-mediated proteolysis after release from telomeres, Genes Dev. 17 (2003) 1328–1333.
[6] N.W. Kim, M.A. Piatyszek, K.R. Prowse, et al., Specific association of human telomerase activity with immortal cells and cancer, Science 266 (1994) 2011–2015.
[7] J.W. Shay, S. Bacchetti, A survey of telomerase activity in human cancer, Eur. J. Cancer 33 (1997) 787–791.
[8] B.S. Herbert, G.C. Gellert, A. Hochreiter, et al., Lipid modification of GRN163, an N3' → P5' thio-phosphoramidate oligonucleotide, enhances the potency of telomerase inhibition, Oncogene 24 (2005) 5262–5268.
[9] H. Seimiya, T. Oh-hara, T. Suzuki, et al., Telomere shortening and growth inhibition of human cancer cells by novel synthetic telomerase inhibitors MST-312, MST-295, and MST-1991, Mol. Cancer Ther. 1 (2002) 657–665.
[10] N. McCabe, M.A. Cerone, T. Ohishi, et al., Therapeutic application: a therapeutic strategy for BRCA-associated cancer, Oncogene 28 (2009) 1465–1470.
[11] H.E. Bryant, N. Schultz, H.D. Thomas, et al., Specific killing of BRCA2-deficient tumours with inhibitors of poly(ADP-ribose) polymerase, Nature 434 (2005) 913–917.
[12] H. Farmer, N. McCabe, C.J. Lord, et al., Targeting the DNA repair defect in BRCA mutant cells as a therapeutic strategy, Nature 434 (2005) 917–921.
[13] S.M. Huang, Y.M. Mishina, S. Liu, et al., Tankyrase inhibition stabilizes axin and antagonizes Wnt signalling, Nature 461 (2009) 614–620.
[14] N. Goshima, Y. Kawamura, A. Fukumoto, et al., Human protein factory for converting the transcriptome into an in vitro-expressed proteome, Nat. Methods 5 (2008) 1011–1017.
[15] A. Matsuyama, A. Shirai, Y. Yashiroda, et al., pDUAL, a multipurpose, multicopy vector capable of chromosomal integration in fission yeast, Yeast 21 (2004) 1289–1305.
[16] A. Matsuyama, R. Arai, Y. Yashiroda, et al., ORFeome cloning and global analysis of protein localization in the fission yeast Schizosaccharomyces pombe, Nat. Biotechnol. 24 (2006) 841–847.
[17] S. Moreno, A. Klar, P. Nurse, Molecular genetic analysis of fission yeast Schizosaccharomyces pombe, Methods Enzymol. 194 (1991) 795–823.
[18] K. Nishi, M. Yoshida, M. Nishimura, et al., A leptomycin B resistance gene of Schizosaccharomyces pombe encodes a protein similar to the mammalian P-glycoproteins, Mol. Microbiol. 6 (1992) 761–769.
[19] K. Nagao, Y. Taguchi, M. Arioka, et al., bfr1$^+$, a novel gene of Schizosaccharomyces pombe which confers brefeldin A resistance, is structurally related to the ATP-binding cassette superfamily, J. Bacteriol. 177 (1995) 1536–1543.
[20] C. Lo, D. Kaida, S. Nishimura, et al., Inhibition of splicing and nuclear retention of pre-mRNA by spliceostatin A in fission yeast, Biochem. Biophys. Res. Commun. 364 (2008) 573–577.
[21] A. Shirai, A. Matsuyama, Y. Yashiroda, et al., Global analysis of gel mobility of proteins and its use in target identification, J. Biol. Chem. 283 (2008) 10745–10752.
[22] T. Ohishi, T. Tsuruo, H. Seimiya, Evaluation of tankyrase inhibition in whole cells, Methods Mol. Enzymol. 194 (1991) 133–146.
[23] L. Geraets, H.J.J. Moonen, K. Brauers, et al., Flavone as PARP-1 inhibitor: its effect on lipopolysaccharide induced gene-expression, Eur. J. Pharmacol. 573 (2007) 241–248.
[24] E. Perkins, D. Sun, A. Nguyen, et al., Novel inhibitors of poly(ADP-ribose) polymerase/PARP1 and PARP2 identified using a cell-based screen in yeast, Cancer Res. 61 (2001) 4175–4183.
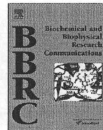
Functional availability of γ-herpesvirus K-cyclin is regulated by cellular CDK6 and p16INK4a

Hidenori Yoshioka [a], Kohji Noguchi [a,*], Kazuhiro Katayama [a], Junko Mitsuhashi [a], Satoshi Yamagoe [b], Masahiro Fujimuro [c], Yoshikazu Sugimoto [a]

[a] Division of Chemotherapy, Faculty of Pharmacy, Keio University, 1-5-30 Shiba-koen, Minato-ku, Tokyo 105-8512, Japan
[b] Department of Bioactive Molecules, National Institute of Infectious Diseases, 1-23-1 Toyama, Shinjuku-ku, Tokyo 162-8640, Japan
[c] Department of Molecular Cell Biology, Interdisciplinary Graduate School of Medicine and Engineering, University of Yamanashi, 1110 Shimokato, Chuo, Yamanashi 409-3898, Japan

ABSTRACT

Viral K-cyclin derived from Kaposi's sarcoma-associated herpesvirus is homologous with mammalian D-type cyclins. Here, we demonstrated the regulatory mechanisms for K-cyclin function and degradation in human embryonic kidney HEK293 and primary effusion lymphoma JSC-1 cell lines. Proteasome inhibitor MG132 treatment induced an accumulation of ubiquitinated K-cyclin in these cells, and co-expression of CDK6 prevented K-cyclin ubiquitination. Also K-cyclin mutants incompetent for CDK6-binding were destabilized by proteasome pathway. Furthermore, silencing of p16INK4a promoted K-cyclin–CDK6 complex formation and hence induced K-cyclin-associated kinase activity in HEK293 cells. These observations indicate that CDK6-bound K-cyclin is functionally stable but monomeric K-cyclin is targeted to ubiquitin-dependent degradation pathway in these cells. Our data suggest that the balance between CDK6 and p16INK4a regulates the availability of functional K-cyclin in human cells.

© 2010 Elsevier Inc. All rights reserved.

1. Introduction

Kaposi's sarcoma-associated herpesvirus (KSHV/HHV-8) and Epstein-Barr virus (EBV/HHV-4) are both classified as γ-herpesviruses associated with malignancy. These viruses can manipulate host cell processes and deregulate cellular signaling to promote cell growth and survival [1].

KSHV-associated cell transformation involves the viruses' latent cycle; the main latent genes of KSHV are LANA (ORF73), K-cyclin (ORF72) and vFLIP (ORF71). These genes have been shown to manipulate host cell processes [1–3]. LANA can inactivate RB and p53, similar to other oncogenic viral proteins, and enhance E2F activity to promote S phase entry [4,5]. LANA also manipulates GSK-3β to regulate β-catenin activity and Wnt signaling [6,7]. vFLIP is structurally related to cellular FLIP, and is primarily associated with activation of the NF-κB pathway and anti-apoptotic signaling [8,9].

K-cyclin is thought to be involved in the cell cycle transition [10,11]. K-cyclin is a homolog of mammalian D-type cyclins, particularly cyclin D2 (32% identity and 54% similarity). Similar to cellular D-type cyclins, K-cyclin can form complexes predominantly

with CDK6 [12], and the K-cyclin–CDK6 complex can phosphorylate RB protein [10]. The K-cyclin–CDK6 complex have broader substrate specificity than cellular cyclin D–CDK6 and can phosphorylate CDK2 substrates such as ORC1, CDC6, p27Kip1, histone H1, Bcl-2 and p53 [13–15]. In the presence of wild-type p53, K-cyclin expression sensitizes primary cells to various apoptotic stimuli [16], whereas K-cyclin transgenic mice showed lymphomagenesis in the absence of p53 [17], suggesting the malignant potential of K-cyclin in vivo.

The cellular cyclin–CDK complexes are usually regulated by their inhibitors called CDK inhibitor (CKI) [18]. The Cip/Kip family of CKIs binds stoichiometrically to the cyclin and CDK subunit [19]. Interestingly, in vitro studies showed that the K-cyclin–CDK6 complex is resistant to p27Kip1 and p21Cip1 [11] and can inactivate p27Kip1 and p21Cip1 by phosphorylation [20,21]. p27Kip1 and p21Cip1 regulate cellular cyclin–CDK1/2 members during the cell cycle transition. Therefore, the K-cyclin–CDK6 complex may contribute to cyclin-CDK1/2 activation during cell cycle progression by eliminating the inhibitory activities of p27Kip1 and p21Cip1.

Another CKI, the INK4 family, suppresses cellular D-type cyclin-dependent CDK activity. The INK4 family can bind to the cyclin D–CDK4/6 complex to form a ternary complex [22]. Although initial studies reported that the K-cyclin–CDK6 complex was resistant to p16INK4a [11], and that the K-cyclin–CDK6 complex was constitutively active in KSHV-infected BC3 cells [23], other later studies indicated that the unphosphorylated K-cyclin–CDK6 complex is

inhibited by the INK4 family member [22,24,25]. These studies suggest that the basal activity of unphosphorylated CDK6 bound to K-cyclin is strong enough to elicit its activities, but the INK4 family can inhibit the unphosphorylated K-cyclin–CDK6 complex.

Currently, it remains unclear whether K-cyclin-associated proteins can regulate intracellular K-cyclin availability. Here, we showed that CDK6-free K-cyclin was targeted to the ubiquitin-dependent destabilization pathway in human cells. We also showed that p16INK4a silencing stimulated intracellular K-cyclin–CDK6 complex formation. These data suggest that the functional availability of K-cyclin is largely dependent on the balance in expression between cellular CDK6 and p16INK4a.

2. Materials and methods

2.1. Plasmids

cDNA for K-cyclin was amplified from the genomic DNA fraction of BCBL cells by standard PCR methods and subcloned into the pIRESpuro plasmid (TAKARA Bio Inc., Shiga, Japan) to construct a C-terminal FLAG-HA-tagged K-cyclin. The murine mutant v-cyclins K104E and E133V were unable to form a complex with cellular CDK4/6 [26]. The mutant K-cyclins K106E and E135V, which have highly conserved amino acid sequences corresponding to v-cyclins K104E and E133V, respectively, were generated using a PCR-based QuikChange™ site-directed mutagenesis kit (Agilent Technologies, Stratagene, La Jolla, CA, USA). Synthetic primers for E135V (5′-GAACTTATAGACCAGGTGAAAGAACTCCTTGAGAAG-3′ and 5′-CTTCT CAAGGAGTTCTTTCACCTGGTCTATAAGTTC-3′) and K106E (5′-CTGTT AGTGCCCAGTGAGCTCAGAAGCCTCACGCC-3′ and 5′-GGCGTGAGGC TTCTGAGCTCACTGGCCACTAACAG-3′) were used with the template pIRESpuro/K-cyclin–FH plasmid. cDNA for CDK6 was amplified by PCR using a HeLa cDNA library and subcloned into the pD3HA plasmid (pcDNA3-modified expression plasmid) to construct a C-terminal myc-tagged CDK6. The LANA-expressing pcDNA3/LANA and histidine-tagged ubiquitin expressing pcDNA3/His-Ub were generated as previously described [27,28].

2.2. Cell culture and transfection

HEK293, BC3 and JSC-1 (from ATCC) cells were cultured in Dulbecco's modified Eagle's or RPMI1640 medium (Sigma–Aldrich, St. Louis, MO, USA) supplemented with 7% fetal bovine serum and kanamycin (50 μg/mL) at 37 °C in 5% CO₂. To establish the K-cyclin transfectants, HEK293 cells were transfected with the expression plasmid using FuGENE® HD transfection reagents (Roche Diagnostics GmbH, Mannheim, Germany). The mixed populations selected by puromycin (0.5 μg/mL) were designated as 293/K-cyclin, 293/ E135V and 293/K106E. 293/LANA was established after screening of G418-resistant pcDNA3/LANA-transfected clones. Full-length LANA expression was confirmed by Western blotting. LANA and K-cyclin co-expressing cells were established by transfection of the K-cyclin plasmid into 293/LANA cells, and the G418- and puromycin-resistant mixed population was designated as 293/LANA + K-cyclin cells.

For siRNA experiments, cells were transfected with siRNA using Lipofectamine™ 2000 (Life Technologies Corp., Invitrogen, Carlsbad, CA, USA). Control scramble (AllStars negative control) and p16INK4a-targeted (Hs_CDKN2A_15) siRNAs were purchased from Qiagen (Hilden, Germany).

2.3. Western blotting

Cells were lysed in SDS buffer (50 mM Tris–HCl [pH 8.0], 2% SDS and 10% glycerol) and sonicated. Other soluble cell extracts were prepared using NEB100 lysis buffer, and SDS–PAGE and Western

blotting were performed as previously described [29]. Western blotting signals were detected using an ECL-Plus chemiluminescence detection kit (Amersham Biosciences, Piscataway, NJ, USA) or a Super Signal West Dura Extended Duration Substrate (Thermo Fisher Scientific Inc., Pierce, Rockford, IL, USA). Anti-HA (3F10) and anti-c-myc (9E10) monoclonal antibodies were purchased from Roche Diagnostics (Indianapolis, IN, USA). Anti-CDK6 and anti-p16INK4a antibodies were from Santa Cruz Biotechnology Inc. (Santa Cruz, CA, USA), and anti-GAPDH antibody was from Millipore Corp., Chemicon (Billerica, MA, USA). Anti-LANA antibody was from Advanced Biotechnologies Inc. (Columbia, MD, USA).

2.4. Nickel–NTA–agarose purification

Transfected cells were lysed in 1 mL of buffer A (8 M urea, 0.1 M Na₂HPO₄–NaH₂PO₄ [pH 8.0], 0.3 M NaCl and 10 mM imidazole) per sample at 48 h after transfection. The lysate was sonicated for 1 min to reduce viscosity and then mixed on a rotator with 10 μL of nickel–NTA–agarose (Qiagen) for 2 h at room temperature. The beads were washed three times with 250 μL of buffer A, twice with 250 μL of buffer A diluted 1:4 with buffer B (25 mM Tris–HCl [pH 6.8] and 20 mM imidazole), and twice with 250 μL of buffer B. Purified proteins were eluted with buffer C (0.1 M EDTA and 250 mM imidazole). The proteins were analyzed by Western blotting.
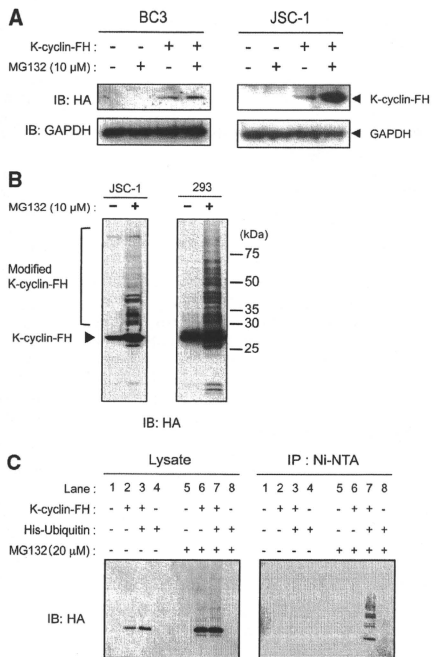
2.5. Immunoprecipitation and in vitro immunocomplex kinase assay

Transfected cells were lysed on ice for 5 min in NEB100 lysis buffer. The cleared cell lysates were subjected to immunoprecipitation with anti-FLAG M2 affinity gel (Sigma–Aldrich). The immunocomplexes were eluted with 0.2 mg/mL of FLAG peptide (Sigma–Aldrich). The phosphorylation reaction was performed in a buffer containing 50 mM Tris–HCl (pH 7.5), 10 mM MgCl₂, 1 mM dithiothreitol, 100 μM ATP and 10 μCi [γ-³²P]ATP with 5 μL of the eluted proteins. The reactions were stopped by the addition of 4× Laemmli SDS sample buffer, resolved by SDS–PAGE and analyzed with a FLA 7000 fluoro image analyzer (Fujifilm, Tokyo, Japan).
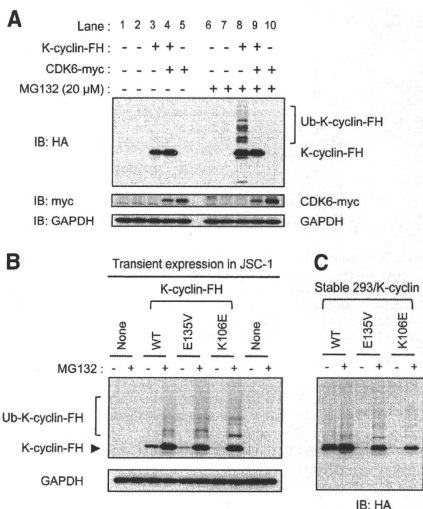
3. Results

3.1. Ubiquitination of K-cyclin

Previous studies suggested that K-cyclin is not a substrate for ubiquitination [23,30]. We also found that the viral K-cyclin protein level in BC3 cells was unaffected by the proteasome inhibitor MG132 treatment (data not shown). However, ubiquitination of K-cyclin itself remains unclear. To confirm it in other cells, we expressed exogenous K-cyclin tagged with FLAG and HA at the C-terminus (K-cyclin–FH) in another line of KSHV-infected cells because JSC-1 cells did not express a detectable level of K-cyclin. To our surprise, the K-cyclin–FH protein level was increased in JSC-1 cells after MG132 treatment, but not in BC3 cells (Fig. 1A). In addition, MG132 treatment induced the expression of the high-molecular weight K-cyclin–FH protein in JSC-1 and HEK293 cells (Fig. 1B). Since MG132 inhibits ubiquitin-dependent proteasomal degradation, the high-molecular weight K-cyclin–FH was considered to be a polyubiquitinated protein. To test this hypothesis, K-cyclin–FH and histidine-tagged ubiquitin (His-Ub) were co-expressed in HEK293 cells to isolate the His-Ub-conjugated protein. MG132 treatment induced the accumulation of the high-molecular weight K-cyclin–FH protein (Fig. 1C, left panel, lanes 6 and 7). Importantly, K-cyclin–FH protein was detected in the His-Ub-conjugated sample collected after MG132 treatment using Ni–NTA beads (Fig. 1C, right panel, lane 7). Thus, these data indicate that K-cyclin was subjected to ubiquitination at least in JSC-1 and HEK293 cells, but probably not in BC3 cells.

A BC3 / JSC-1

K-cyclin-FH : - - + + / - - + +
MG132 (10 µM) : - + - + / - + - +

IB: HA

IB: GAPDH

◄ K-cyclin-FH

GAPDH

B

JSC-1 / 293

MG132 (10 µM) : - + / - +

(kDa)
—75
—50
—35
—30
—25

Modified K-cyclin-FH

K-cyclin-FH ►

IB: HA

C   Lysate   IP : Ni-NTA

Lane : 1 2 3 4   5 6 7 8   1 2 3 4   5 6 7 8
K-cyclin-FH : - + + -   - + + -   - + + -   - + + -
His-Ubiquitin : - - + +   - - + +   - - + +   - - + +
MG132(20 µM) : - - - -   + + + +   - - - -   + + + +

IB: HA

Fig. 1. Ubiquitination of K-cyclin in cells. (A) Transiently expressed K-cyclin–FH in BC3 and JSC-1 cells in the presence or absence of MG132 (10 µM for 6 h) was detected by Western blotting (IB) with anti-HA antibody. The expression of GAPDH protein is shown as a loading control. (B) Transiently expressed K-cyclin–FH with or without MG132 treatment was detected by Western blotting. Chemiluminescence signals were recorded with a long exposure to visualize the high-molecular weight K-cyclin–FH protein. High-molecular weight K-cyclin–FH is indicated as modified K-cyclin–FH, and the arrow indicates the normal K-cyclin–FH signal. (C) K-cyclin–FH was transiently co-expressed in HEK293 cells with His-Ub in the presence or absence of MG132, and His-Ub-conjugated protein was collected by Ni–NTA agarose (IP: Ni–NTA). Western blotting using anti-HA antibody showed K-cyclin–FH protein in the lysate sample (left panel) and in the His-Ub-conjugated sample (right panel).

A

Lane : 1 2 3 4 5   6 7 8 9 10

K-cyclin-FH : - - + + -   - - + + -
CDK6-myc : - - - + +   - - - + +
MG132 (20 µM) : - - - - -   + + + + +

IB: HA

Ub-K-cyclin-FH

K-cyclin-FH

IB: myc

CDK6-myc

IB: GAPDH

GAPDH

B   Transient expression in JSC-1   **C**

K-cyclin-FH   Stable 293/K-cyclin

None / WT / E135V / K106E / None   WT / E135V / K106E

MG132 : - + - + - + - + - +   - + - + - +

Ub-K-cyclin-FH

K-cyclin-FH ►

GAPDH

IB: HA

Fig. 2. CDK6-binding prevents K-cyclin ubiquitination. K-cyclin–FH and CDK6-myc were transiently expressed in HEK293 cells with or without MG132 treatment (A). Wild-type (WT) and CDK-free mutant (E135V and K106E) K-cyclin–FH proteins were transiently expressed in KSHV-infected JSC-1 cells (B), or stably expressed in puromycin-selected HEK293 cells (C). High-molecular weight ubiquitinated K-cyclin–FH proteins (Ub–K-cyclin–FH) were detected after MG132 treatment (10 µM in JSC-1 cells or 20 µM in HEK293 cells for 6 h) by Western blotting using an anti-HA antibody (IB: HA).

sion levels of mutant E135V and K106E were lower than that of wild-type K-cyclin–FH in JSC-1 cells, even though the same expression vector was used for plasmid construction (Fig. 2B). Moreover, these differences in protein expression were overcome by MG132 treatment (Fig. 2B, E135V and K106E). These observations were confirmed using stable HEK293 transfectant cells expressing mutant K-cyclins. The expression levels of the mutant E135V and K106E K-cyclin–FH were much lower in the stable cell lines than that of wild-type K-cyclin–FH (Fig. 2C, MG132–). MG132 treatment dramatically increased the expression of mutant K-cyclin–FH proteins and Ub–K-cyclin–FH in these stable cell lines (Fig. 2C, MG132+). These observations suggest that K-cyclin needs to interaction with CDK to escape from ubiquitin-dependent degradation, and that CDK-free K-cyclin would be targeted to ubiquitination in these cells. Collectively, an interaction with CDK6 seems to be a determinant for ubiquitination and the stability of K-cyclin in HEK293 cells and JSC-1 cells.

3.3. K-cyclin associates with CDK6 and p16INK4a in HEK293 cells

To explore other factor(s) affecting K-cyclin-dependent activity, K-cyclin–FH was purified from stably K-cyclin–FH-expressing 293/K-cyclin cells by a tandem affinity chromatography method using anti-FLAG and anti-HA antibody agaroses. Silver staining after SDS–PAGE showed that a few proteins (major bands of 45, 36 and 15 kDa) were stably co-purified with K-cyclin–FH (∼29 kDa) (Fig. 3A). The 45-kDa band seemed to be nonspecific because it was also detected in the control extract from parental HEK293 cells. Previous studies suggest that K-cyclin can form a complex with CDK and CKIs [10,11]. According to their estimated molecular

3.2. K-cyclin is stabilized by forming a complex with CDK

Because K-cyclin preferentially forms a complex with CDK6 intracellularly, we examined the effect of CDK6 co-expression on the ubiquitination of K-cyclin. As described above, high-molecular weight polyubiquitinated K-cyclin–FH (Ub–K-cyclin–FH) accumulated in HEK293 cells treated with MG132 (Fig. 2A, lane 8). However, when CDK6 was co-expressed, the accumulation of Ub–K-cyclin–FH was clearly abolished (Fig. 2A, lane 9). These data suggest that complex formation with CDK6 would prevent K-cyclin from undergoing ubiquitination. To test this hypothesis, we prepared K-cyclin–FH mutants, E135V-FH and K106E-FH, containing single amino acid substitutions. Crystal structural analysis and functional studies have shown that K106 and E135 in K-cyclin, and the corresponding K104 and E133 in homologous murine v-cyclin, are important for binding to CDK6 and that amino acid substitution of these residues reduced CDK6-binding [25,26,31]. Transient expression experiments showed that the protein expres-
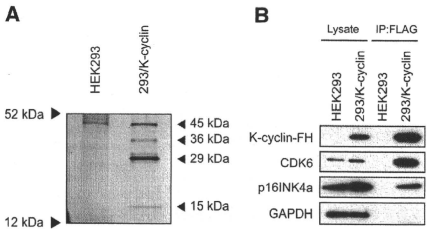
Fig. 3. K-cyclin forms a complex with CDK6 and p16INK4a in HEK293 cells. (A) K-cyclin–FH complex sequentially immunopurified with anti-FLAG and anti-HA agaroses were visualized after SDS–PAGE and silver staining. (B) CDK6 and p16INK4a proteins in the K-cyclin–FH immunocomplex were confirmed by Western blotting. The left lanes (lysate) were input lysate samples and the right lanes (IP: FLAG) were immunopurified samples.

weights, these 36- and 15-kDa proteins appeared to be CDKs and CKIs, respectively. Western blotting detected CDK6 and p16INK4a in the K-cyclin–FH immunocomplex (Fig. 3B). Because p16INK4a binds directly to CDK6, the K-cyclin–CDK6–p16INK4a heterotrimer is formed in HEK293 cells.

3.4. K-cyclin-dependent kinase activity is suppressed by p16INK4a in HEK293 cells

Previous *in vitro* studies strongly suggested that the kinase activity of the K-cyclin–CDK6 complex is resistant to p16INK4a [11]. Therefore, we re-examined whether its association with p16INK4a plays no role in the regulation of the K-cyclin–CDK6 complex activity in cells. RNA interference experiments were performed to knockdown p16INK4a protein, and reduction of p16INK4a was validated by Western blotting (Fig. 4A). Scramble (control) and p16INK4a-targeted siRNA did not suppress the expression of other proteins, such as CDK6 and K-cyclin. The K-cyclin–FH complex was immunopurified by anti-FLAG antibody agarose from either control- or p16INK4a-knockdown cells, and Western blotting of immunopurified samples indicated that the K-cyclin–FH immunocomplex from p16INK4a-knockdown cells contained higher amounts of CDK6 and lower amounts of p16INK4a than that from control siRNA-treated cells (Fig. 4B). Then, an *in vitro* immunocomplex kinase assay was performed to examine its kinase activity using GST-RB (amino acids 701–928) as a substrate (Fig. 4C). The immunocomplex from K-cyclin–FH-expressing cells showed GST-RB phosphorylation activities, while those from parental HEK293 cells did not. As was expected, the kinase activity of the K-cyclin–FH complex from p16INK4a-knockdown cells was apparently stronger (about fivefold) than that
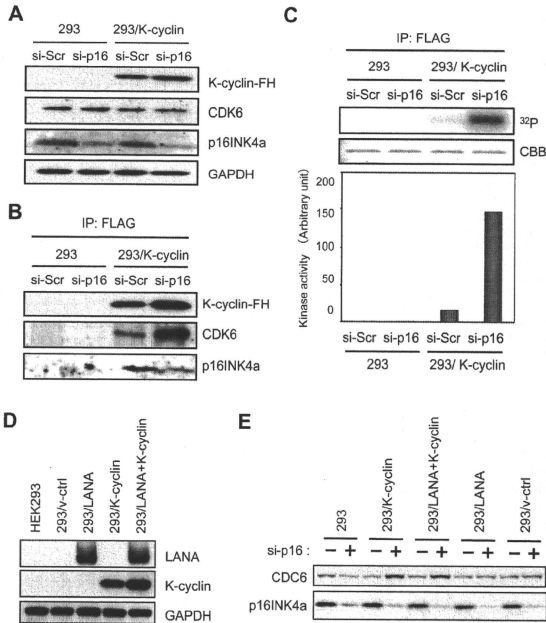
Fig. 4. Intracellular kinase activity of the K-cyclin complex is regulated by p16INK4a. (A) Protein expressions in the parental (293) and stable K-cyclin–FH-expressing (293/K-cyclin) cells after transfection of either control scramble (si-Scr) or p16INK4a-targeted siRNA (si-p16) for 2 days. (B) CDK6 and p16INK4a proteins were analyzed in the K-cyclin–FH immunocomplex collected by anti-FLAG antibody agarose (IP: FLAG) from the siRNA-treated cells used in (A). (C) The *in vitro* immunocomplex kinase assay was performed using GST-RB (amino acids 701–982) protein as a substrate. CBB indicates coomassie blue staining of GST-RB in the gel as a control, and phosphorylation (32P) was detected with the FLA 7000 system. (D) The expression of LANA and K-cyclin–FH in the stable HEK293 cell lines was detected by Western blotting. (E) The K-cyclin–FH- and LANA-expressing stable cell lines were transfected or not with p16INK4a-targeted siRNA for 2 days and CDC6 and p16INK4a protein expression was detected by Western blotting.

from control siRNA-treated cells. These data indicated that the formation and activity of the K-cyclin–CDK6 complex would be induced after intracellular depletion of p16INK4a. To confirm this, we established HEK293 cell lines that stably expressed viral proteins such as LANA, K-cyclin, or LANA and K-cyclin (Fig. 4D), and Western blotting was used to detect the expression of putative targets of the K-cyclin–CDK6 complex. CDC6 was reported to be phosphorylated by the K-cyclin–CDK6 complex in an in vitro kinase assay [32] and was induced by transduction of K-cyclin into normal human cells [33]. In our assay, p16INK4a-knockdown selectively increased CDC6 protein expression in the K-cyclin–FH-expressing cell lines (Fig. 4E). These data suggest that cellular p16INK4a can inhibit K-cyclin-dependent kinase activity by inhibiting K-cyclin–CDK6 complex formation in human cells.

4. Discussion

K-cyclin is structurally similar to cyclin D and forms a ternary complex with CDK6 and INK4. In this study, we found that CDK-free K-cyclin was targeted to the ubiquitin-dependent proteasome pathway, which was inhibited by CDK6 overexpression. We also showed that knockdown of p16INK4a stimulated the formation of the K-cyclin–CDK6 complex. These observations suggest that the balance between CDK6 and p16INK4a regulates the functional availability of K-cyclin.

Cellular D-type cyclins are regulated by ubiquitin-dependent degradation pathway. GSK-3β-mediated phosphorylation at the C-terminus was shown to alter the subcellular localization and proteasomal turnover of cyclin D1 and D2 [34], and SCF (Fbx4-αB crystallin) was identified as a ubiquitin E3 ligase for phosphorylated cyclin D1 [35]. Distinct from cellular cyclins, K-cyclin lacks a typical degron and the half-life of the K-cyclin protein was reported to be longer than that of other cellular cyclins in KSHV-infected BC3 cells [23]. Thus K-cyclin was thought to be free from the ubiquitin-dependent destabilization. However, we showed that MG132 induced the accumulation of ubiquitinated K-cyclin protein in HEK293 and JSC-1 cells. Although these data may contradict earlier studies, we confirmed that the expression of K-cyclin in BC3 cells was not affected by MG132 treatment. Therefore, the ubiquitin-dependent mechanism regulating K-cyclin protein might be cell-type specific, or some types of cells, such as BC3 cells, might lack a component necessary for K-cyclin destabilization because a significant amount of K-cyclin protein was detected in BC3 cells, but not in JSC-1 cells. It might be interesting to look at other KSHV-infected cells in terms of K-cyclin stability and ubiquitination. Identification of the K-cyclin destabilization system is needed to confirm these inconsistencies between cell types. We also found that the protein levels of mutant K-cyclins that lost their CDK-binding ability was apparently lower than that of the wild-type K-cyclin, and were restored by MG132 treatment. Our data suggest that the interaction with CDK6 would prevent the ubiquitination of K-cyclin and, therefore, only the monomeric K-cyclin might be targeted to the ubiquitin–proteasome degradation system in cells. Interestingly, a previous study showed similar observations that CDK-free cyclin D1 can be ubiquitinated independently of its phosphorylation on Thr-286 [36]. Therefore, a, currently unknown, mechanism is likely to regulate the ubiquitination of CDK-free K- or D-cyclin in cells.

The cyclin D–CDK6 complex is sensitive to the INK4 family, and the ternary formation of the K-cyclin–CDK6–p18INK4c complex induces a conformational change in CDK6, which interferes with ATP-binding and the alignment of catalytic residues, resulting in the inactivation of this complex [22]. However, the regulatory impact of INK4 on the efficacy of the K-cyclin–CDK6 complex formation in vivo has been unclear. We observed that knockdown of p16INK4a increased the association between CDK6 and K-cyclin.

The INK4 family proteins bind directly to monomeric CDK4/6, and INK4-binding distorts the cyclin-binding site of CDK4/6, which weakens the affinity of cyclin for CDK4/6, preventing its association with cyclin D [18]. Thus, we presume that the binding of p16INK4a to CDK6 would interfere with K-cyclin-binding to CDK6. These observations suggest that cellular INK4a not only directly inhibits the dimeric K-cyclin–CDK6, but also represses the initiation of K-cyclin–CDK6 complex formation, suggesting that p16INK4a will determine the efficiency of K-cyclin-binding to CDK6 in cells. As some KSHV-infected cell lines, including BC3 cells, lost p16INK4a expression [37], such inactivation of negative regulators of K-cyclin will contribute to the stable activity of K-cyclin in KSHV-infected cells.

Acknowledgments

References

[1] C. Boshoff, Y. Chang, Kaposi's sarcoma-associated herpesvirus: a new DNA tumor virus, Annu. Rev. Med. 52 (2001) 453–470.

[2] P.S. Moore, Y. Chang, Kaposi's sarcoma-associated herpesvirus immunoevasion and tumorigenesis: two sides of the same coin?, Annu Rev. Microbiol. 57 (2003) 609–639.

[3] S.C. Verma, E.S. Robertson, Molecular biology and pathogenesis of Kaposi sarcoma-associated herpesvirus, FEMS Microbiol. Lett. 222 (2003) 155–163.

[4] J. Friborg Jr., W. Kong, M.O. Hottiger, G.J. Nabel, P53 inhibition by the LANA protein of KSHV protects against cell death, Nature 402 (1999) 889–894.

[5] S.A. Radkov, P. Kellam, C. Boshoff, The latent nuclear antigen of Kaposi sarcoma-associated herpesvirus targets the retinoblastoma-E2F pathway and with the oncogene Hras transforms primary rat cells, Nat. Med. 6 (2000) 1121–1127.

[6] M. Fujimuro, F.Y. Wu, C. APRhys, H. Kajumbula, D.B. Young, G.S. Hayward, S.D. Hayward, A novel viral mechanism for dysregulation of beta-catenin in Kaposi's sarcoma-associated herpesvirus latency, Nat. Med. 9 (2003) 300–306.

[7] M. Fujimuro, S.D. Hayward, Manipulation of glycogen-synthase kinase-3 activity in KSHV-associated cancers, J. Mol. Med. 82 (2004) 223–231.

[8] M. Thome, P. Schneider, K. Hofmann, H. Fickenscher, E. Meinl, F. Neipel, C. Mattmann, K. Burns, J.L. Bodmer, M. Schroter, C. Scaffidi, P.H. Krammer, M.E. Peter, J. Tschopp, Viral FLICE-inhibitory proteins (FLIPs) prevent apoptosis induced by death receptors, Nature 386 (1997) 517–521.

[9] L. Liu, M.T. Eby, N. Rathore, S.K. Sinha, A. Kumar, P.M. Chaudhary, The human herpesvirus 8-encoded viral FLICE inhibitory protein physically associates with and persistently activates the Ikappa B kinase complex, J. Biol. Chem. 277 (2002) 13745–13751.

[10] D. Godden-Kent, S.J. Talbot, C. Boshoff, Y. Chang, P. Moore, R.A. Weiss, S. Mittnacht, The cyclin encoded by Kaposi's sarcoma-associated herpesvirus stimulates cdk6 to phosphorylate the retinoblastoma protein and histone H1, J. Virol. 71 (1997) 4193–4198.

[11] C. Swanton, D.J. Mann, B. Fleckenstein, F. Neipel, G. Peters, N. Jones, Herpes viral cyclin/Cdk6 complexes evade inhibition by CDK inhibitor proteins, Nature 390 (1997) 184–187.

[12] M. Li, H. Lee, D.W. Yoon, J.C. Albrecht, B. Fleckenstein, F. Neipel, J.U. Jung, Kaposi's sarcoma-associated herpesvirus encodes a functional cyclin, J. Virol. 71 (1997) 1984–1991.

[13] E.W. Verschuren, N. Jones, G.I. Evan, The cell cycle and how it is steered by Kaposi's sarcoma-associated herpesvirus cyclin, J. Gen. Virol. 85 (2004) 1347–1361.

[14] P.M. Ojala, K. Yamamoto, E. Castanos-Velez, P. Biberfeld, S.J. Korsmeyer, T.P. Makela, The apoptotic v-cyclin–CDK6 complex phosphorylates and inactivates Bcl-2, Nat. Cell Biol. 2 (2000) 819–825.

[15] P.C. Chang, M. Li, Kaposi's sarcoma-associated herpesvirus K-cyclin interacts with Cdk9 and stimulates Cdk9-mediated phosphorylation of p53 tumor suppressor, J. Virol. 82 (2008) 278–290.

[16] E.W. Verschuren, J Klefstrom, G.I. Evan, N. Jones, The oncogenic potential of Kaposi's sarcoma-associated herpesvirus cyclin is exposed by p53 loss in vitro and in vivo, Cancer Cell 2 (2002) 229–241.

[17] E.W. Verschuren, J.G. Hodgson, J.W. Gray, S. Kogan, N. Jones, G.I. Evan, The role of p53 in suppression of KSHV cyclin-induced lymphomagenesis, Cancer Res. 64 (2004) 581–589.

[18] C.J. Sherr, J.M. Roberts, CDK inhibitors: positive and negative regulators of G1-phase progression, Genes Dev. 13 (1999) 1501–1512.

[19] A.A. Russo, P.D. Jeffrey, A.K. Patten, J. Massague, N.P. Pavletich, Crystal structure of the p27Kip1 cyclin-dependent-kinase inhibitor bound to the cyclin A–Cdk2 complex, Nature 382 (1996) 325–331.
[20] D.J. Mann, E.S. Child, C. Swanton, H. Laman, N. Jones, Modulation of p27(Kip1) levels by the cyclin encoded by Kaposi's sarcoma-associated herpesvirus, EMBO J. 18 (1999) 654–663.
[21] A. Jarviluoma, E.S. Child, G. Sarek, P. Sirimongkolkasem, G. Peters, P.M. Ojala, D.J. Mann, Phosphorylation of the cyclin-dependent kinase inhibitor p21Cip1 on serine 130 is essential for viral cyclin-mediated bypass of a p21Cip1-imposed G1 arrest, Mol. Cell. Biol. 26 (2006) 2430–2440.
[22] P.D. Jeffrey, L. Tong, N.P. Pavletich, Structural basis of inhibition of CDK–cyclin complexes by INK4 inhibitors, Genes Dev. 14 (2000) 3115–3125.
[23] R. Van Dross, S. Yao, S. Asad, G. Westlake, D.J. Mays, L. Barquero, S. Duell, J.A. Pietenpol, P.J. Browning, Constitutively active K-cyclin/cdk6 kinase in Kaposi sarcoma-associated herpesvirus-infected cells, J. Natl. Cancer Inst. 97 (2005) 656–666.
[24] P. Kaldis, P.M. Ojala, L. Tong, T.P. Makela, M.J. Solomon, CAK-independent activation of CDK6 by a viral cyclin, Mol. Biol. Cell 12 (2001) 3987–3999.
[25] U. Schulze-Gahmen, S.H. Kim, Structural basis for CDK6 activation by a virus-encoded cyclin, Nat. Struct. Biol. 9 (2002) 177–181.
[26] J.W. Upton, L.F. van Dyk, S.H. Speck, Characterization of murine gammaherpesvirus 68 v-cyclin interactions with cellular cdks, Virology 341 (2005) 271–283.
[27] Y. Murakami, S. Yamagoe, K. Noguchi, Y. Takebe, N. Takahashi, Y. Uehara, H. Fukazawa, Ets-1-dependent expression of vascular endothelial growth factor receptors is activated by latency-associated nuclear antigen of Kaposi's sarcoma-associated herpesvirus through interaction with Daxx, J. Biol. Chem. 281 (2006) 28113–28121.
[28] K. Noguchi, A. Kokubu, C. Kitanaka, H. Ichijo, Y. Kuchino, ASK1-signaling promotes c-Myc protein stability during apoptosis, Biochem. Biophys. Res. Commun. 281 (2001) 1313–1320.
[29] K. Noguchi, A. Vassilev, S. Ghosh, J.L. Yates, M.L. DePamphilis, The BAH domain facilitates the ability of human Orc1 protein to activate replication origins in vivo, EMBO J. 25 (2006) 5372–5382.
[30] R. Van Dross, P.J. Browning, J.C. Pelling, Do truncated cyclins contribute to aberrant cyclin expression in cancer?, Cell Cycle 5 (2006) 472–477.
[31] P. Kaldis, The N-terminal peptide of the Kaposi's sarcoma-associated herpesvirus (KSHV)-cyclin determines substrate specificity, J. Biol. Chem. 280 (2005) 11165–11174.
[32] H. Laman, D. Coverley, T. Krude, R. Laskey, N. Jones, Viral cyclin–cyclin-dependent kinase 6 complexes initiate nuclear DNA replication, Mol. Cell. Biol. 21 (2001) 624–635.
[33] S. Koopal, J.H. Furuhjelm, A. Jarviluoma, S. Jaamaa, P. Pyakurel, C. Pussinen, M. Wirzenius, P. Biberfeld, K. Alitalo, M. Laiho, P.M. Ojala, Viral oncogene-induced DNA damage response is activated in Kaposi sarcoma tumorigenesis, PLoS Pathog. 3 (2007) 1348–1360.
[34] J.A. Diehl, F. Zindy, C.J. Sherr, Inhibition of cyclin D1 phosphorylation on threonine-286 prevents its rapid degradation via the ubiquitin-proteasome pathway, Genes Dev. 11 (1997) 957–972.
[35] D.I. Lin, O. Barbash, K.G. Kumar, J.D. Weber, J.W. Harper, A.J. Klein-Szanto, A. Rustgi, S.Y. Fuchs, J.A. Diehl, Phosphorylation-dependent ubiquitination of cyclin D1 by the SCF(FBX4-alphaB crystallin) complex, Mol. Cell 24 (2006) 355–366.
[36] D. Germain, A. Russell, A. Thompson, J. Hendley, Ubiquitination of free cyclin D1 is independent of phosphorylation on threonine 286, J. Biol. Chem. 275 (2000) 12074–12079.
[37] G. Platt, A. Carbone, S. Mittnacht, p16INK4a loss and sensitivity in KSHV associated primary effusion lymphoma, Oncogene 21 (2002) 1823–1831.

BCRP/ABCG2 confers anticancer drug resistance without covalent dimerization

Junichi Shigeta, Kazuhiro Katayama, Junko Mitsuhashi, Kohji Noguchi and Yoshikazu Sugimoto[1]

Division of Chemotherapy, Faculty of Pharmacy, Keio University, Tokyo, Japan

In previous studies, we demonstrated that the breast cancer resistance protein (BCRP, ABCG2) forms an S–S homodimer. The BCRP-C603S mutant substituting Ser for Cys-603 in the third extracellular domain formed both a 70–75-kDa monomer and 140–150-kDa dimer, suggesting that Cys-603 is an important residue in the covalent bridge. These results also suggested the involvement of other Cys residues in dimer formation. In the present study, we examined the possible involvement of the other extracellular Cys residues, Cys-592 and Cys-608, in the dimerization and transporter functions of BCRP using double and triple Cys-mutant BCRP transfectants. In SDS–PAGE under non-reducing conditions, BCRP-C592S·C603S and BCRP-C592S·C608S were detected as dimers whereas BCRP-C603S·C608S and BCRP-C592S·C603S·C608S were found only as monomers. This finding indicated that no Cys residues other than the three extracellular Cys are responsible for the dimer formation. The formation of BCRP-C592S·C603S dimer suggested the involvement of Cys-608 in the covalent linkage of this mutant BCRP. PA/C592S·C603S·C608S-cl.7 cells showed a significant level of multiple drug resistance and low-level accumulation of mitoxantrone. These results clearly demonstrate that BCRP functions as a drug resistance protein without covalent dimerization. Among drug-resistant Cys-mutant BCRP transfectants, PA/C603S, PA/C592S·C608S, and PA/C592S·C603S·C608S were found to be more resistant to the reversal effects of fumitremorgin C than PA/WT, suggesting some alteration in the substrate recognition in Cys-mutant BCRPs. In conclusion, Cys-mediated covalent dimerization is not required for BCRP to function as a transporter. In addition to Cys-603, Cys-608 may also be involved in BCRP dimer formation. (Cancer Sci 2010; 101: 1813–1821)

C ancer cells that acquire resistance to certain chemotherapeutic agents sometimes develop cross-resistance to structurally unrelated drugs. This phenomenon is known as multidrug resistance. ATP-binding cassette (ABC) transporters such as P-glycoprotein and multidrug resistance-associated protein 1 (MRP1) have an internally duplicated structure with two transmembrane domains and two ATP-binding domains. These proteins pump out various structurally unrelated anticancer agents in an energy-dependent manner. Thus cells expressing these transporters manifest a multidrug-resistant phenotype.[1–5] In contrast, breast cancer resistance protein (BCRP/ABCG2/MXR) is a half transporter, possessing a C-terminal transmembrane domain and an N-terminal ATP-binding domain.[6–9] Breast cancer resistance protein (BCRP) mediates the resistance of various anticancer drugs such as 7-ethyl-10-hydroxycamptothecin (SN-38), which is an active metabolite of irinotecan, topotecan, and mitoxantrone, by pumping out them out of cells.[6–14]

We have previously shown that BCRP forms a homodimer bridged by disulfide bonds.[15] To identify Cys residues that are involved in dimerization and explore the role of the covalent binding in protein activity, we performed cysteine-scanning mutagenesis substituting Ser for Cys. We established 12 transfectants expressing Cys-mutant BCRPs. Among these,

BCRP-C603S mutant substituting Ser for Cys-603 was found to migrate both as a 70–75-kDa monomer and as a 140–150-kDa dimer in SDS–PAGE under non-reducing conditions.[16] The PA/C603S transfectant showed the drug resistance phenotype. Cys-603 is located in the third extracellular domain (between the 5th and 6th transmembrane domains) of BCRP, which comprises 62 amino acids (Fig. 1). This suggested that Cys-603 is an important residue in the formation of the covalent bridge between BCRP monomers. However, the existence of a small amount of 150-kDa dimer in the PA/C603S transfectant suggested the involvement of other Cys residues in this process. In addition, it was unclear whether this non-covalently bound BCRP really functions as a drug efflux pump. Two other cysteine residues (Cys-592 and Cys-608) are also present in this same domain (Fig. 1). These are candidates that would participate in BCRP dimer formation.

In the present study, to elucidate the possible involvement of Cys-592 and Cys-608 in BCRP dimerization and protein activity, we established double (C592S·C603S, C592S·C608S, and C603S·C608S) and triple (C592S·C603S·C608S) mutant BCRP transfectants, and compared the expression, protein formation, and function of these BCRP mutants with wild-type and single (C592S, C603S, and C608S) mutant proteins.

Materials and Methods

Mutant BCRP transfectants. Double (C592S·C603S, C592S·C608S, and C603S·C608S) and triple (C592S·C603-S·C608S) mutant BCRP cDNAs were generated using a site-directed mutagenesis kit (Takara Bio, Otsu, Japan), according to the manufacturer's instructions. The mutant BCRP cDNAs were cloned into pHa-IRES-DHFR bicistronic expression vector harboring a mutant dihydrofolate reductase (DHFR) cDNA under the control of an internal ribosome entry site (IRES). The wild-type and single (C592S, C603S, and C608S) mutant BCRP cDNAs in the same vector were also used as controls.[16] Murine fibroblast PA317 cells were transfected with the mutant BCRP vectors as described previously.[16] The transfected cells were then selected with 120 ng/mL methotrexate for 8 days. The resulting methotrexate-resistant cells were mixed and used as mixed populations of transfectants. Clonal cells were obtained from the mixed populations of transfectants by a standard limiting dilution technique. The mutant BCRP cDNAs in the transfectants were amplified by PCR and the nucleotide sequences were confirmed by direct sequencing.

Western blot analysis. Cell lysates from the BCRP transfectants were prepared in the presence or absence of 5% 2-mercaptoethanol as described previously,[16] resolved using 5–20% SDS–PAGE (5 μg of protein per lane, unless specified), and then electro-transferred onto nitrocellulose membranes. The membranes were incubated with 1 μg/mL of rabbit anti-BCRP

[1]To whom correspondence should be addressed.
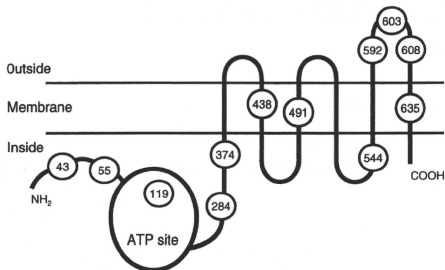E-mail: sugimoto-ys@pha.keio.ac.jp

Fig. 1. Schematic depiction of the breast cancer resistance protein (BCRP) with 12 cysteine residues indicated. Three of these residues, Cys-592, Cys-603, and Cys-608, are localized in the third extracellular domain.

polyclonal antibody 3488[15] and/or mouse anti-GAPDH monoclonal antibody (Chemicon, Temecula, CA, USA). This was followed by washing and treatment with peroxidase-conjugated sheep antirabbit and/or antimouse IgGs (Amersham, Buckinghamshire, UK), respectively. The membrane-bound antibodies were visualized using an enhanced chemiluminescence detection system (Amersham).

Growth inhibition assay. The sensitivity of the mutant *BCRP* transfectants to anticancer agents was evaluated using cell growth inhibition assays after incubation of the cells for 4 days at 37°C in the presence or absence of various concentrations of anticancer agents. Cell numbers were determined with a Coulter counter (Beckman Coulter, Brea, CA, USA). The IC_{50} value (the drug dose causing a 50% inhibition of cell growth) was determined from growth inhibition curves, and the degree of resistance (x-fold) was calculated by dividing the IC_{50} values of the *BCRP* transfectants by those of the parental PA317 cells. The effects of fumitremorgin C (FTC), a BCRP inhibitor, were also examined.[17,18] The reversal index (RI) was determined by dividing the degree of resistance in the absence of FTC by the degree of resistance in the presence of FTC.

Intracellular accumulation of mitoxantrone. The intracellular accumulation of mitoxantrone in the mutant *BCRP* transfectants was determined by flow cytometry. Cells (5×10^5) were incubated in the presence or absence of 1 μM mitoxantrone for 40 min at 37°C and then washed and resuspended in ice-cold phosphate-buffered saline (PBS). Fluorescence was determined using a BD LSR II flow cytometer (Becton, Dickinson and Company, Franklin Lakes, NJ, USA).

Immunofluorescent microscopy. PA317 or *BCRP* transfectants were seeded onto Lab-Tek II chamber slides (5×10^4 cells/1.7 cm²-well; Nalge Nunc International, Naperville, IL, USA) and cultured overnight. The cells were fixed with 4% paraformaldehyde for 15 min at room temperature, washed with PBS three times, and then permeabilized with 0.5% Triton X-100 in PBS for 15 min at room temperature. After washing the cells with PBS three times, non-specific binding sites were blocked with 3% bovine serum albumin (BSA)/PBS for 15 min at room temperature. Cells were then incubated with 2.5 μg/mL of mouse anti-BCRP monoclonal antibody BXP-21 (Chemicon) for 60 min at room temperature. After washing cells with PBS three times, the cells were incubated with 1 μg/mL of an Alexa Fluor 488 goat antimouse antibody (Molecular Probes, Eugene, OR, USA) for 30 min at room temperature, washed with PBS three times and mounted in a Prolong Gold antifade reagent with DAPI (Invitrogen, Carlsbad, CA, USA). Acquisition of images was performed using FV1000-D confocal microscopy (Olympus, Tokyo, Japan).

Results

Establishment of mutant *BCRP* transfectants. PA317 cells were transfected with the wild-type, single (C592S, C603S, and C608S), double (C592S·C603S, C592S·C608S, and C603S·C608S), and triple (C592S·C603S·C608S) mutant *BCRP* cDNAs in Pha-IRES-DHFR bicistronic expression vector as described previously.[16] In cells transfected with Pha-BCRP-IRES-DHFR, a single mRNA is transcribed under the control of a retroviral LTR promoter, and two gene products are translated independently from a bicistronic mRNA. Cells expressing mutant DHFR show a high-level resistance to methotrexate. The transfected cells were therefore selected with 120 ng/mL methotrexate for 8 days. The resulting mixed populations of the drug-selected cells were designated as PA/WT-mix, PA/C592S-mix, PA/C603S-mix, PA/C608S-mix, PA/C592S·C603S-mix, PA/C592S·C608S-mix, PA/C603S·C608S-mix, and PA/C592S·C603S·C608S-mix. Nine clonal cells were established from each of these mixed populations by limiting dilution.

Expression of mutant *BCRP* in mixed populations of transfected cells. The BCRP expression levels in the mixed populations of methotrexate-selected cells were evaluated by western blot analysis under reducing conditions (Fig. 2a). Wild-type BCRP and BCRP-C603S both migrated as a 75-kDa molecule. BCRP-C592S·C603S migrated as 75-kDa and 70-kDa species. Other BCRP mutants migrated mostly as a 70-kDa molecule. A high level of BCRP expression was observed in PA/WT-mix, PA/C603S-mix, and PA/C592S·C608S-mix cells (Fig. 2a).
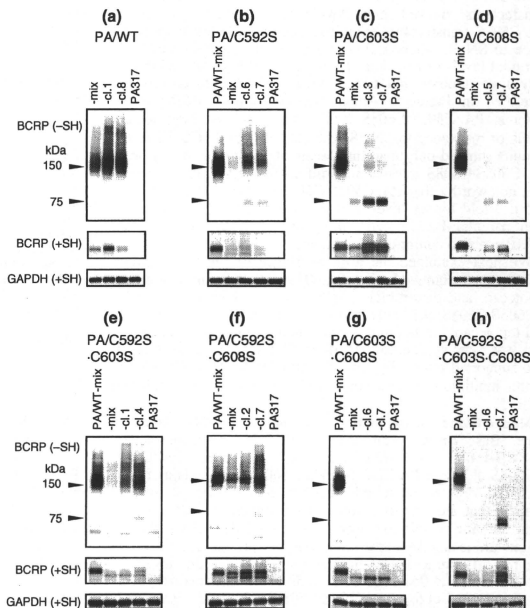
Breast cancer resistance protein (BCRP) dimerization in each of the PA317 transfectants was evaluated by western blotting under non-reducing conditions (Fig. 2b). As reported previously, BCRP-C603S migrated as both a 150-kDa dimer and a 70–75-kDa monomer. Breast cancer resistance protein (BCRP) dimer formation was observed in PA/WT-mix, PA/C592S-mix, PA/C592S·C603S-mix, and PA/C592S·C608S-mix cells. The BCRP expression levels in PA/C608S-mix, PA/C603S·C608S-mix, and PA/C592S·C603S·C608S-mix cells were too low to evaluate dimer/monomer formation (Fig. 2b).

Expression of mutant *BCRP* in mutant *BCRP* transfectant clones. Since BCRP expression of PA/C592S·C603S·C608S-mix cells was low, we next isolated the mutant *BCRP* transfectant clones. Western blot analyses of all of the clones are shown in Figure S1. Figure 3 shows the BCRP expression profiles for the selected clones, together with PA/WT and the corresponding mixed populations. The BCRP expression levels and dimer/dimer formation in PA/WT and single mutant *BCRP* transfectants (PA/C592S, PA/C603S, and PA/C608S) were essentially the same as those in our previous report (Fig. 3a–d).[16] Among double mutant *BCRP* transfectants, BCRP dimer formation was prominent in PA/C592S·C603S and PA/C592S·C608S cells (Fig. 3e,f). In contrast, monomer formation in these transfectants was marginal, although single mutation in Cys-603 or Cys-608 resulted in monomer formation. It should be noted that BCRP-C592S·C603S formed a BCRP dimer in the absence of Cys-603. Another double mutant *BCRP* transfectant, PA/C603S·C608S, expressed a small amount of BCRP monomer (Fig. 3g). As shown in Figure 3(h), a triple mutant *BCRP* transfectant, PA/C592S·C603S·C608S-cl.7, expressed a fairly high level of the BCRP monomer. No dimer formation was evident in this cell line. This finding indicated that the three extracellular Cys residues, Cys-592, Cys-603, and/or Cys-608, are responsible for BCRP dimer formation. It was also suggested that dimer formation of BCRP-C592S·C603S might be due to the involvement of Cys-608 in the covalent linkage of this mutant BCRP.

Two species of BCRP, 75-kDa and 70-kDa, were detected in western blot analyses under reducing conditions (Fig. 3). The
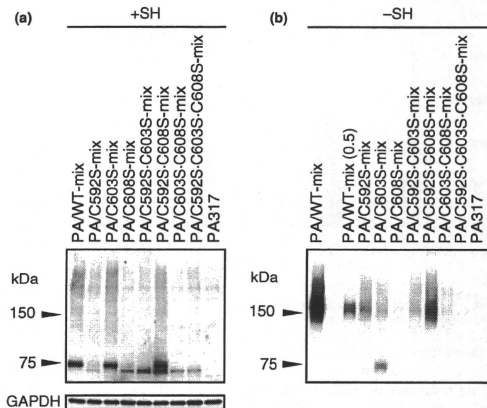
Fig. 2. Expression of mutant breast cancer resistance protein (BCRP) in mixed populations of transfected cells. (a) Western blot analysis was performed under reducing (+SH) conditions. GAPDH expression was analyzed as an internal control of protein loading in reducing conditions. (b) Western blot analysis was performed under non-reducing (−SH) conditions. In lane PA/WT-mix(0.5), 0.5 µg protein was loaded on SDS–PAGE.

Fig. 3. Expression of mutant breast cancer resistance protein (BCRP) in selected transfectant clones. Breast cancer resistance protein (BCRP) expression in a mixed population of cells (-mix) and in two transfectant clones with relatively high BCRP expression (-cl.X) was examined. PA/WT-mix was used as a control cell line. Western blot analysis was performed under reducing (+SH) and non-reducing (−SH) conditions. GAPDH expression was analyzed as an internal control of protein loading in reducing conditions. (a) PA/WT cells; (b) PA/C592S cells; (c) PA/C603S cells; (d) PA/C608S cells; (e) PA/C592S·C603S cells; (f) PA/C592S·C608S cells; (g) PA/C603S·C608S cells; (h) PA/C592S·C603S·C608S cells.

relative expression levels of 75-kDa and 70-kDa BCRP in transfectants to the PA/WT-mix cells were calculated from each BCRP band under reducing conditions (Fig. 3) and are presented in Figure 4. PA/WT cells expressed 75-kDa BCRP only, and PA/C603S cells mostly expressed the 75-kDa molecule.

The ratio of 75-kDa BCRP in PA/C592S, PA/C592S·C608S, and PA/C592S·C603S·C608S cells was two-third to half of the total BCRP. The expression levels of 70-kDa BCRP were higher than those of 75-kDa BCRP in other transfectants, especially PA/C603S·C608S cells.
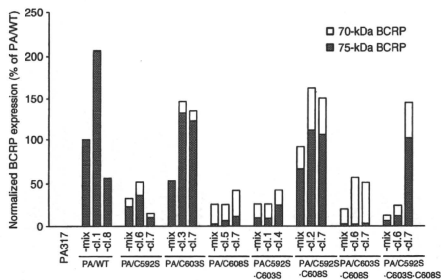
Fig. 4. Normalized breast cancer resistance protein (BCRP) expression in transfectant clones. The relative expression levels of total and 75-kDa BCRP in transfectants as compared with PA/WT-mix cells were calculated from each BCRP band under reducing conditions (Fig. 3).

Legend: □ 70-kDa BCRP ■ 75-kDa BCRP

Y-axis: Normalized BCRP expression (% of PA/WT)

Table 1. SN-38 resistance of mutant *BCRP* transfectants

Cell line	IC$_{50}$ to SN-38† (nM)	Degree of resistance‡ (x-fold)	Relative expression level Total BCRP§	75-kDa BCRP¶
PA317	3.7 ± 0.2	1	–	–
PA/WT-mix	90 ± 4.4	24	100	100
PA/WT-cl.1	172 ± 6.1	47	207	206
PA/WT-cl.8	77 ± 10.3	21	56	56
PA/C592S-mix	12.4 ± 0.8	3.4	34	24
PA/C592S-cl.6	28.5 ± 1.4	7.7	52	37
PA/C592S-cl.7	13.7 ± 0.5	3.7	16	11
PA/C603S-mix	9.7 ± 0.5	2.6	54	51
PA/C603S-cl.3	409 ± 15.9	110	146	132
PA/C603S-cl.7	158 ± 17.7	43	135	122
PA/C608S-mix	4.8 ± 0.3	1.3	27	3
PA/C608S-cl.5	5.6 ± 0.2	1.5	26	7
PA/C608S-cl.7	6.3 ± 0.6	1.7	43	12
PA/C592S·C603S-mix	3.6 ± 0.2	1.0	27	10
PA/C592S·C603S-cl.1	5.1 ± 1.1	1.4	27	10
PA/C592S·C603S-cl.4	6.2 ± 0.8	1.7	43	26
PA/C592S·C608S-mix	16.7 ± 1.8	4.6	92	67
PA/C592S·C608S-cl.2	22.8 ± 2.0	6.2	163	111
PA/C592S·C608S-cl.7	34.5 ± 4.9	9.4	151	106
PA/C603S·C608S-mix	2.9 ± 0.2	0.8	21	3
PA/C603S·C608S-cl.6	4.4 ± 0.4	1.2	57	3
PA/C603S·C608S-cl.7	3.4 ± 0.1	0.9	51	4
PA/C592S·C603S·C608S-mix	4.1 ± 0.2	1.1	13	7
PA/C592S·C603S·C608S-cl.6	4.0 ± 0.4	1.1	25	13
PA/C592S·C603S·C608S-cl.7	11.1 ± 1.5	3.0	145	102

†The cells were incubated for 4 days at 37°C in the presence or absence of various concentrations of 7-ethyl-10-hydroxycamptothecin (SN-38). The IC$_{50}$ value (the drug dose causing a 50% inhibition of cell growth) was determined from growth inhibition curves. Data are the mean ± SD from triplicate determinations. ‡The degree of resistance (x-fold) was calculated by dividing the IC$_{50}$ values of the breast cancer resistance protein (*BCRP*) transfectants by those of the parental PA317 cells. §Each total BCRP (75- and 70-kDa) band intensity was measured (Fig. 3), and the relative expression levels were calculated by dividing BCRP expression values in each cell line as compared with PA/WT-mix cells. ¶Each 75-kDa BCRP band intensity (not including 70-kDa band) was measured (Fig. 3), and the relative expression levels were calculated by dividing BCRP expression values in each cell line compared with PA/WT-mix cells.

Drug resistance of mutant *BCRP* transfectants. The effects of substituting Ser for Cys in BCRP on cellular drug resistance were evaluated using a cell growth inhibition assay. The SN-38 resistance levels of mutant *BCRP* transfectant sublines are listed in Table 1. PA/WT, PA/C603S-cl.3, and PA/C603S-cl.7 transfectants showed high levels of resistance to SN-38. PA/C592S transfectants exhibited intermediate levels of resistance to SN-38 whereas PA/C608S transfectants showed only marginal levels of resistance to this drug. The growth inhibition curves of double- and triple-mutant *BCRP* transfectants are described in Figure 5. Among double mutant *BCRP* transfectants, PA/C592S·C608S transfectants showed intermediate levels of resistance to SN-38 whereas PA/C592S·C603S transfectants showed only marginal levels of resistance to this drug. PA/C603S·C608S transfectants did not show SN-38 resistance. It is noteworthy that PA/C592S·C603S·C608S-cl.7 cells exhibited a 3-fold higher level of resistance to SN-38 as compared with parental PA317 cells, indicating that this triple-mutant BCRP can also confer drug resistance.

We next examined the drug resistance of the triple-mutant *BCRP* transfectant, PA/C592S·C603S·C608S, to mitoxantrone, topotecan, and doxorubicin. As shown in Figure 6, PA/C592-S·C608S-cl.7 cells showed resistance to mitoxantrone and topotecan, but not to doxorubicin. This cross-resistance pattern was very similar to that of PA/WT-mix cells. This result also supported our finding that BCRP-C592S·C603S·C608S can confer multiple drug resistance similar to that of the wild-type BCRP.

Mitoxantrone accumulation in mutant *BCRP* transfectants. Based on the results of drug sensitivity assay, we selected PA/WT-mix, PA/C592S-cl.6, PA/C603S-cl.3, PA/C592-S·C608S-cl.7, and PA/C592S·C603S·C608S-cl.7 cells as representative drug-resistant transfectants for further study. To confirm that the drug resistance of the mutant *BCRP* transfectants was attributable to a lowered accumulation of the drug, a mitoxantrone uptake experiment was performed. As shown in Figure 7(a), intracellular mitoxantrone was at low levels in PA/WT-mix and PA/C603S-cl.3 cells and at intermediate levels in PA/C592S-cl.6, PA/C592S·C608S-cl.7, and PA/C592-S·C603S·C608S-cl.7 cells. These data were in good agreement with the results of the drug sensitivity assay. Fluorescence-activated cell sorter (FACS) fluorograms of mitoxantrone accumulation experiments are shown in Figure S2.

To confirm that BCRP-C592S·C603S·C608S expression caused lowered accumulation of mitoxantrone, we then performed a mitoxantrone accumulation assay in *BCRP*-knocked down PA/C592S·C603S·C608S-cl.7 cells (Fig. 7c). PA317 and

PA/WT-mix cells were also used in this experiment as negative and positive controls, respectively. Breast cancer resistance protein (BCRP) small-interfering RNA (siRNA) was found to suppress both wild-type BCRP and BCRP-C592S·C603S·C608S expression (Fig. 7b). In PA317 cells, *BCRP* siRNA hardly affected intracellular mitoxantrone levels. Again, intracellular mitoxantrone levels in PA/WT-mix and PA/C592S·C603-S·C608S-cl.7 cells transfected with control siRNA was much lower than that in PA317 cells. Transfection with *BCRP* siRNA restored intracellular mitoxantrone levels in both PA/WT-mix and PA/C592S·C603S·C608S-cl.7 cells. In particular, intracellular mitoxantrone in PA/C592S·C603S·C608S-cl.7 cells transfected with *BCRP* siRNA was present at almost the same level as that in PA317 cells. These results suggest that lower level occurrence of intracellular mitoxantrone depends on BCRP expression in both PA/WT-mix and PA/C592S·C603S·C608S-cl.7 cells. Fluorescence-activated cell sorter (FACS) fluorograms of mitoxantrone accumulation experiments are shown in Figure S3.

Localization of mutant BCRP in mutant *BCRP* transfectants. Immunofluorescent microscopy analysis using an anti-BCRP antibody BXP-21 was performed to examine whether
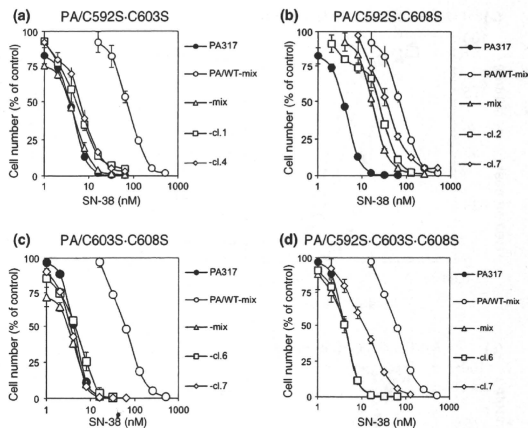
(a) PA/C592S·C603S

(b) PA/C592S·C608S

(c) PA/C603S·C608S

(d) PA/C592S·C603S·C608S

BCRP-C592S·C603S·C608S is expressed on the cell surface. As shown in Figure 8, wild-type BCRP expression was detected predominantly on the cell surface. In contrast, only a small amount of BCRP-C592S·C603S·C608S was expressed on the surface of the transfectant, and most of the triple mutant BCRPs was present in the cytoplasm. Subcellular localization of other mutant BCRPs in the transfectants is shown in Figure S4.

Effect of FTC on SN-38 and mitoxantrone resistance of the mutant BCRP transfectants. To examine the sensitivity of mutant BCRPs to a BCRP inhibitor, namely FTC, the reversal effect of FTC on the mutant BCRP transfectants was examined. PA/C603S-cl.7 was added to the panel of drug-resistant transfectants in this experiment. As shown in Table 2, FTC (1 μM) completely reversed the resistance of PA/WT-mix and PA/C603S-cl.6 cells to SN-38 and mitoxantrone. Fumitremorgin C (FTC) reversed the drug resistance of PA/C603S-cl.3 and PA/C603S-cl.7 cells, although these cells still showed 4- to 15-fold higher levels of resistance to SN-38 and mitoxantrone in the presence of FTC. Fumitremorgin C (FTC) slightly lowered the resistance of PA/C592S·C608S-cl.7 cells to SN-38, but did not affect their resistance to mitoxantrone. Fumitremorgin C (FTC) had no effect on the resistance of PA/C592S·C603S·C608S-cl.7 cells to SN-38 and mitoxantrone (Table 2). These results demonstrate that substitution of Cys residues in the extracellular domain of BCRP alters the sensitivity of the transporter to FTC.

Discussion

We have previously reported that Cys-603 is an important residue in the formation of the covalent bridge between BCRP monomers.[16] In the present study, we generated cells expressing double (C592S·C603S, C592S·C608S, and C603S·C608S) and triple (C592S·C603S·C608S) mutant BCRP transfectants. We employed the bicistronic vector pHa-BCRP-IRES-DHFR, which allows for the direct selection of transfected cells with methotrexate.[19–22] We have shown in a previous study that mixed populations of Cys mutant BCRP-transfected cells express similar levels of exogenous BCRP mRNA.[16] We used the same strategy in our current study. However, as shown in Figure 2,

some of the mixed population of the transfected cells expressed very low amounts of mutant BCRP. We therefore isolated mutant BCRP transfectant clones to obtain cells that highly expressed the exogenous mutant protein to evaluate BCRP dimerization and the resistance levels of the cells to anticancer agents.

Consistent with our previous study, PA/C603S cells expressed both monomeric and dimeric BCRP.[16] PA/C608S cells also expressed a BCRP monomer whereas PA/C592S cells expressed a BCRP dimer. The triple-mutant BCRP transfectant, PA/C592S·C603S·C608S-cl.7, expressed a BCRP monomer only. This indicated that the three extracellular Cys residues, Cys-592, Cys-603, and/or Cys-608, are responsible for BCRP dimer formation, and that no other Cys residue is involved. Among double mutant BCRP transfectants, PA/C592S·C603S and PA/C592S·C608S expressed BCRP dimers, but PA/C603S·C608S expressed only a BCRP monomer. It has been discussed by Henriksen et al.[23] that an intramolecular disulfide bridge exists between Cys-592 and Cys-608. From this discussion and the findings of our study, we propose disulfide-binding modes in wild-type and mutant BCRPs. Free Cys-603 is normally allowed to configure a homodimer of BCRP. Single mutation on Cys-603 loses this homo-dimerization site, and it can therefore be concluded that BCRP-C603S protein mainly existed as a monomer. The intramolecular disulfide bridge between Cys-592 and Cys-608 is partially disrupted for some reason, and small amount of the BCRP dimer could be detected in PA/C603S. Introduction of the C592S mutation into BCRP-C603S extinguishes the counter partner against Cys-608 in the intramolecular disulfide bridge. As a result, free Cys-608 is produced and dimerization of BCRP may be restored via this site. Double mutant BCRP on Cys-603 and Cys-608 has no more dimerization sites, and thus this mutant is thought to exist as a monomer. In PA/C608S cells, Cys-603 can also construct an intramolecular disulfide bridge with Cys-592, and therefore a single mutation on Cys-608 may weaken dimerization of BCRP. The above scheme is illustrated in Figure S5. Altogether, Cys-608 in addition to Cys-603, but not Cys-592, is involved in the dimerization of BCRP.

We successfully demonstrated that the triple-mutant BCRP, namely BCRP-C592S·C603S·C608S, functions as an active transporter whose expression confers drug resistance. In a
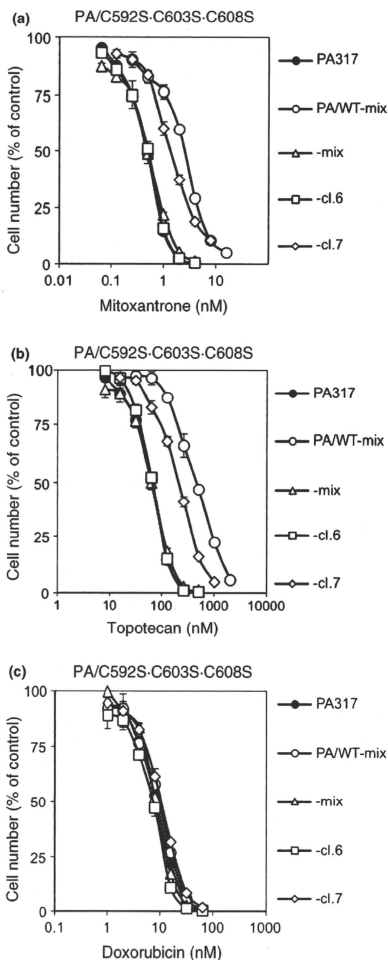
Fig. 6. Cross-resistance pattern of triple-mutant breast cancer resistance protein (*BCRP*) transfectants. The cells were incubated for 4 days at 37°C in the presence or absence of various concentrations of mitoxantrone, topotecan, or doxorubicin. Cell numbers were determined with a Coulter counter. Data are the mean ± SD of triplicate determinations. PA317 and PA/WT-mix were used as control cell lines. (a) Mitoxantrone resistance in PA/C592S·C603S·C608S cells. (b) Topotecan resistance in PA/C592S·C603S·C608S cells. (c) Doxorubicin resistance in PA/C592S·C603S·C608S cells.

Fig. 7. Mitoxantrone accumulation in mutant breast cancer resistance protein (*BCRP*) transfectants. (a) Cells (5 × 10⁵) were incubated in the presence or absence of 1 μM mitoxantrone for 40 min at 37°C and then washed and resuspended in ice-cold PBS. Fluorescence was determined by flow cytometry. Bars indicate median channels of fluorescence in the transfectants. (1) PA317 cells; (2) PA/WT-mix cells; (3) PA/C592S-cl.6 cells; (4) PA/C603S-cl.3 cells; (5) PA/C592S·C608S-cl.7 cells; (6) PA/C592S·C603S·C608S-cl.7 cells. (b) Cells were seeded onto 60 mm dishes (2 × 10⁵ cells/dish) and cultured overnight. Cells were transfected with non-silencing control or *BCRP* siRNA using Lipofectamine 2000. Western blot analysis was performed under non-reducing conditions (–SH). GAPDH expression was analyzed as an internal control of protein loading. (c) The mitoxantrone accumulation assay was performed in siRNA-transfected cells as described in (a). (1) PA317 cells transfected with control siRNA. (2) PA317 cells transfected with *BCRP* siRNA. (3) PA/WT-mix cells transfected with control siRNA. (4) PA/WT-mix cells transfected with *BCRP* siRNA. (5) PA/C592S·C603S·C608S-cl.7 cells transfected with control siRNA. (6) PA/C592S·C603S·C608S-cl.7 cells transfected with *BCRP* siRNA.

previous study Henriksen *et al.*[23] reported a low expression of triple-mutant BCRP, which prevented an evaluation of its functional activity. We also found that the generation of transfectants expressing high levels of the triple-mutant BCRP was somewhat difficult and thus performed the selection of multiple clones. PA/C592S·C603S·C608S-cl.7 cells showed resistance to mitoxantrone and topotecan, but not to doxorubicin (Fig. 5), and a
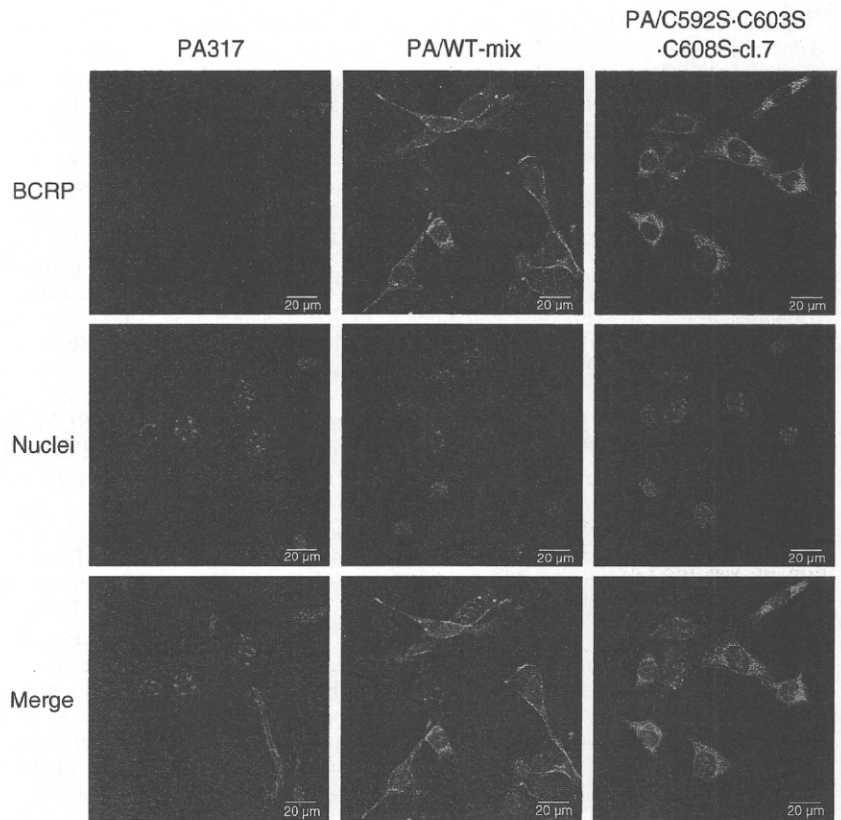
Fig. 8. Localization of breast cancer resistance protein (BCRP) protein in PA/WT and PA/C592S·C603S·C608S cells. The cells were stained with anti-BCRP antibody BXP-21 following an Alexa Fluor 488 goat antimouse antibody (green). Nuclei were stained with DAPI (blue). PA317 cells were also stained with BXP-21 and DAPI as a negative control. Breast cancer resistance protein (*BCRP*) and nuclei were observed using confocal microscopy.

Table 2. Effect of FTC on the SN-38 and mitoxantrone resistance of mutant *BCRP* transfectants

Cell line	SN-38			Mitoxantrone			Relative expression level of total BCRP§
	Degree of resistance†		RI‡	Degree of resistance†		RI‡	
	−FTC	+FTC		−FTC	+ FTC		
PA317	1.0 ± 0.1	0.9 ± 0.1	−	1.0 ± 0.1	0.9 ± 0.1	−	−
PA/WT-mix	19.3 ± 1.7	1.4 ± 0.1	13.8	9.0 ± 0.3	1.2 ± 0.1	7.5	100
PA/C592S-cl.6	4.2 ± 0.3	1.2 ± 0.1	3.5	3.7 ± 0.1	1.3 ± 0.1	2.8	52
PA/C603S-cl.3	106 ± 7.3	7.9 ± 0.3	13.4	57 ± 5.9	15 ± 0.7	3.8	146
PA/C603S-cl.7	18 ± 2.0	4.1 ± 0.2	4.4	28 ± 3.9	12 ± 1.0	2.3	135
PA/C592S·C608S-cl.7	8.4 ± 0.5	4.0 ± 0.2	2.1	3.3 ± 0.2	3.3 ± 0.1	1.0	151
PA/C592S·C603S·C608S-cl.7	4.1 ± 0.3	4.6 ± 0.3	0.9	7.5 ± 0.2	6.0 ± 0.8	1.3	145

†The cells were incubated for 4 days at 37°C in the presence or absence of various concentrations of anticancer agents in the presence or absence of 1 µM fumitremorgin C (FTC). The IC_{50} value (the drug dose causing a 50% inhibition of cell growth) was determined from growth inhibition curves, and the degree of resistance (x-fold) was calculated by dividing the IC_{50} values of the breast cancer resistance protein (*BCRP*) transfectants by those of the parental PA317 cells. ‡The reversal index (RI) was determined by dividing the degree of resistance in the absence of FTC by the degree of resistance in the presence of FTC. Data are the mean ± SD of triplicate determinations. §Each total BCRP (75- and 70-kDa) band intensity was measured (Fig. 3), and the relative expression levels were calculated by dividing BCRP expression values in each cell line as compared with PA/WT-mix cells.

cross-resistance pattern which was very similar to that of the PA/WT-mix cells. We carefully confirmed the complete sequence of the mutant *BCRP* cDNA in PA/C592S·C603-S·C608S-cl.7 cells. The possibility of unexpected additional mutations in this mutant, or contamination of the clonal PA/C592S·C603S·C608S-cl.7 cell culture by wild-type or other mutant BCRP-expressing cells was thus excluded. We concluded that triple-mutant BCRP (BCRP-C592S·C603S·C608S) has some potential to function as a transporter protein and maintains a substrate specificity that is similar to wild-type BCRP with no covalent disulfide bonds. However, our findings do not rule out the possibility that BCRP-C592S·C603S·C608S func-

tions as a dimer or an oligomer without covalent linkages in cells. In this regard, Xu *et al.*[24,25] have reported that BCRP can function as a homo-oligomer via interactions in the third extracellular domain containing the Cys-592, Cys-603, and Cys-608 residues.

PA/WT, PA/C592S, PA/C603S, PA/C592S·C608S, and PA/C592S·C603S·C608S-cl.7 cells exhibited drug resistance and low accumulation of mitoxantrone. PA/WT and PA/C603S cells expressed a 75-kDa BCRP product (Fig. 2). Significant expression of a 75-kDa BCRP was also found in PA/C592S, PA/C592S·C608S, and PA/C592S·C603S·C608S-cl.7 cells, whereas the PA/C608S cells mainly expressed a 70-kDa BCRP

(Fig. 3). The 70-kDa BCRP seems to be an under-molecule. Thus, the expression of a 75-kDa BCRP in these transfectants is likely to be related to the drug resistance phenotype. However, when correlation of SN-38 resistance with both total and 75-kDa BCRP expression levels under reducing conditions was investigated, we found that some mutant BCRP transfectants showed lower drug resistance despite expressing 75-kDa BCRP. This finding suggests that the degree of drug resistance depends on the quality and function of mutant Bcrps rather than on expression levels.

We examined the reversal effects of FTC on the drug resistance levels of wild-type and mutant BCRP transfectants. Fumitremorgin C (FTC) strongly reversed the resistance of PA/WT and PA/C592S cells to SN-38 and mitoxantrone, and partially reversed the drug resistance of PA/C603S cells. However, FTC had no effect on the drug resistance of PA/C592S-C603S-C608S-cl.7 cells. In addition, FTC slightly lowered the resistance of PA/C592S-C608S-cl.7 cells to SN-38, but not to mitoxantrone. These results indicate that a substitution of Ser for Cys in the extracellular domain altered the FTC sensitivity. Similarly, it has been reported that a substitution of Val for Gly in the first intracellular loop of P-glycoprotein alters its substrate specificity and the effects of inhibitors.[26,27]

Breast cancer resistance protein (BCRP) expression has been found in the placenta, intestine, kidney, liver, blood–brain barrier, and hematopoietic stem cells, and is assumed to play a role in the protective functions of such normal tissues against toxic substances and metabolites.[28–30] Competitive inhibitors of BCRP might alter the tissue distribution and blood concentration of substrate anticancer agents. Currently, small molecule tyrosine kinase inhibitors (TKIs) such as imatinib, nilotinib, gefitinib, erlotinib, lapatinib, and sunitinib have been used in various clinical settings. Most of these TKIs are competitive inhibitors for ATP, and good substrates of BCRP and other ABC transporters. We and others have shown that these TKIs strongly inhibit BCRP and sensitize cancer cells to substrate anticancer agents.[31–39] Therefore, co-administration of such TKIs might alter the tissue distribution and blood concentration of substrate anticancer agents.

Functional single nucleotide polymorphisms (SNPs) also appear to be able to alter the expression and function of BCRP. We previously reported that BCRP 421C>A SNP, substituting Lys-141 for Gln, is associated with a low expression of the protein.[40] In a phase I study of diflomotecan, a camptothecin-derivative anticancer agent, patients with a BCRP 421C>A allele had a significantly higher blood concentration of the drug.[41] Cusatis et al.[42] have reported that patients with a BCRP 421C>A allele had a significantly higher risk of developing gefitinib-induced diarrhea. Rudin et al.[43] have demonstrated that the diplotype of two polymorphic loci in the BCRP promoter, involving −15622C>T and 1143C>T, conferred lower BCRP levels associated with higher erlotinib pharmacokinetic parameters, including area under the curve and maximum concentration. We have also reported that two germ line mutations of BCRP in our laboratory, namely 623T>C (F208S) and 1291T>C (F431L), also resulted in the loss of function or severely reduced the function of BCRP.[44] Sunitinib clearly reversed the SN-38 resistance of PA/WT cells but not of BCRP-F431L transfectants. In addition, sunitinib did not inhibit [^{125}I]iodoarylazidoprazosin-binding to BCRP-F431L.[45] Future systematic analyses of the effects of amino acid substitutions on BCRP expression and function will be helpful in furthering our understanding of the structure-function relationship of this protein.

The present study demonstrated that the extracellular Cys residues of BCRP, Cys-603, and Cys-608, are important for the dimer formation of this protein. However, covalent dimerization of BCRP is not necessary for its transporter function. Moreover, substitution of Cys residues in the extracellular domain of BCRP alters the specificity of a specific inhibitor of this transporter.

Acknowledgments

References

1 Gottesman MM, Hrycyna CA, Schoenlein PV, Germann UA, Pastan I. Genetic analysis of the multidrug transporter. *Annu Rev Genet* 1995; **29**: 607–49.
2 Chen CJ, Chin JE, Ueda K *et al.* Internal duplication and homology with bacterial transport proteins in the *mdr1* (P-glycoprotein) gene from multidrug-resistant human cells. *Cell* 1986; **47**: 381–9.
3 Ueda K, Clark DP, Chen CJ, Roninson IB, Gottesman MM, Pastan I. The human multidrug resistance (*mdr1*) gene. cDNA cloning and transcription initiation. *J Biol Chem* 1987; **262**: 505–8.
4 Pastan I, Gottesman MM, Ueda K, Lovelace E, Rutherford AV, Willingham MC. A retrovirus carrying an *MDR1* cDNA confers multidrug resistance and polarized expression of P-glycoprotein in MDCK cells. *Proc Natl Acad Sci USA* 1988; **85**: 4486–90.
5 Cole SP, Bhardwaj G, Gerlach JH *et al.* Overexpression of a transporter gene in a multidrug-resistant human lung cancer cell line. *Science* 1992; **258**: 1650–4.
6 Doyle LA, Yang W, Abruzzo LV *et al.* A multidrug resistance transporter from human MCF-7 breast cancer cells. *Proc Natl Acad Sci USA* 1998; **95**: 15665–70.
7 Allen JD, Brinkhuis RF, Wijnholds J, Schinkel AH. The mouse *Bcrp1/Mxr/Abcp* gene: amplification and overexpression in cell lines selected for resistance to topotecan, mitoxantrone, or doxorubicin. *Cancer Res* 1999; **59**: 4237–41.
8 Ross DD, Yang W, Abruzzo LV *et al.* Atypical multidrug resistance: breast cancer resistance protein messenger RNA expression in mitoxantrone-selected cell lines. *J Natl Cancer Inst* 1999; **91**: 429–33.
9 Maliepaard M, van Gastelen MA, de Jong LA *et al.* Overexpression of the *BCRP/MXR/ABCP* gene in a topotecan-selected ovarian tumor cell line. *Cancer Res* 1999; **59**: 4559–63.

10 Litman T, Brangi M, Hudson E *et al.* The multidrug-resistant phenotype associated with overexpression of the new ABC half-transporter, MXR (ABCG2). *J Cell Sci* 2000; **113**: 2011–21.
11 Kawabata S, Oka M, Shiozawa K *et al.* Breast cancer resistance protein directly confers SN-38 resistance of lung cancer cells. *Biochem Biophys Res Commun* 2001; **280**: 1216–23.
12 Jonker JW, Smit JW, Brinkhuis RF *et al.* Role of breast cancer resistance protein in the bioavailability and fetal penetration of topotecan. *J Natl Cancer Inst* 2000; **92**: 1651–6.
13 Sugimoto Y, Tsukahara S, Ishikawa E, Mitsuhashi J. Breast cancer resistance protein: molecular target for anticancer drug resistance and pharmacokinetics/pharmacodynamics. *Cancer Sci* 2005; **96**: 457–65.
14 Noguchi K, Katayama K, Mitsuhashi J, Sugimoto Y. Functions of the breast cancer resistance protein (BCRP/ABCG2) in chemotherapy. *Adv Drug Deliv Rev* 2009; **61**: 26–33.
15 Kage K, Tsukahara S, Sugiyama T *et al.* Dominant-negative inhibition of breast cancer resistance protein as drug efflux pump through the inhibition of S-S dependent homodimerization. *Int J Cancer* 2002; **97**: 626–30.
16 Kage K, Fujita T, Sugimoto Y. Role of Cys-603 in dimer/oligomer formation of the breast cancer resistance protein BCRP/ABCG2. *Cancer Sci* 2005; **96**: 866–72.
17 Rabindran SK, He H, Singh M *et al.* Reversal of a novel multidrug resistance mechanism in human colon carcinoma cells by fumitremorgin C. *Cancer Res* 1998; **58**: 5850–8.
18 Rabindran SK, Ross DD, Doyle LA, Yang W, Greenberger LM. Fumitremorgin C reverses multidrug resistance in cells transfected with the breast cancer resistance protein. *Cancer Res* 2000; **60**: 47–50.
19 Sugimoto Y, Tsukahara S, Sato S *et al.* Drug-selected co-expression of P-glycoprotein and gp91 in vivo from an *MDR1*-bicistronic retrovirus vector Ha-MDR-IRES-gp91. *J Gene Med* 2003; **5**: 366–76.

20 Sugimoto Y, Aksentijevich I, Gottesman MM, Pastan I. Efficient expression of drug-selectable genes in retroviral vectors under control of an internal ribosome entry site. *Biotechnology* 1994; **12**: 694–8.

21 Sugimoto Y, Hrycyna CA, Aksentijevich I, Pastan I, Gottesman MM. Coexpression of a multidrug-resistance gene (*MDR1*) and *herpes simplex virus* thymidine kinase gene as part of a bicistronic messenger RNA in a retrovirus vector allows selective killing of *MDR1*-transduced cells. *Clin Cancer Res* 1995; **1**: 447–57.

22 Sugimoto Y, Sato S, Tsukahara S *et al*. Coexpression of a multidrug resistance gene (*MDR1*) and *herpes simplex virus thymidine kinase* gene in a bicistronic retroviral vector Ha-MDR-IRES-TK allows selective killing of *MDR1*-transduced human tumors transplanted in nude mice. *Cancer Gene Ther* 1997; **4**: 51–8.

23 Henriksen U, Fog JU, Litman T, Gether U. Identification of intra- and intermolecular disulfide bridges in the multidrug resistance transporter ABCG2. *J Biol Chem* 2005; **280**: 36926–34.

24 Xu J, Liu Y, Yang Y, Bates S, Zhang JT. Characterization of oligomeric human half-ABC transporter ATP-binding cassette G2. *J Biol Chem* 2004; **279**: 19781–9.

25 Xu J, Peng H, Chen Q, Liu Y, Dong Z, Zhang JT. Oligomerization domain of the multidrug resistance-associated transporter ABCG2 and its dominant inhibitory activity. *Cancer Res* 2007; **67**: 4373–81.

26 Choi K, Chen CJ, Kriegler M, Roninson IB. An altered pattern of cross-resistance in multidrug-resistant human cells results from spontaneous mutations in the *mdr1* (P-glycoprotein) gene. *Cell* 1988; **53**: 519–29.

27 Cardarelli CO, Aksentijevich I, Pastan I, Gottesman MM. Differential Effects of P-glycoprotein inhibitors on NIH3T3 cells transfected with wild-type (G185) or mutant (V185) multidrug transporters. *Cancer Res* 1995; **55**: 1086–91.

28 Maliepaard M, Scheffer GL, Faneyte IF *et al*. Subcellular localization and distribution of the breast cancer resistance protein transporter in normal human tissues. *Cancer Res* 2001; **61**: 3458–64.

29 Zhou S, Schuetz JD, Bunting KD *et al*. The ABC transporter Bcrp1/ABCG2 is expressed in a wide variety of stem cells and is a molecular determinant of the side-population phenotype. *Nat Med* 2001; **7**: 1028–34.

30 Jonker JW, Merino G, Musters S *et al*. The breast cancer resistance protein BCRP (ABCG2) concentrates drugs and carcinogenic xenobiotics into milk. *Nat Med* 2005; **11**: 127–9.

31 Yanase K, Tsukahara S, Asada S, Ishikawa E, Imai Y, Sugimoto Y. Gefitinib reverses breast cancer resistance protein–mediated drug resistance. *Mol Cancer Ther* 2004; **3**: 1119–25.

32 Burger H, van Tol H, Boersma AW *et al*. Imatinib mesylate (STI571) is a substrate for the breast cancer resistance protein (BCRP)/ABCG2 drug pump. *Blood* 2004; **104**: 2940–2.

33 Elkind NB, Szentpetery Z, Apati A *et al*. Multidrug transporter ABCG2 prevents tumor cell death induced by the epidermal growth factor receptor inhibitor Iressa (ZD1839, Gefitinib). *Cancer Res* 2005; **65**: 1770–7.

34 McDowell HP, Meco D, Riccardi A *et al*. Imatinib mesylate potentiates topotecan antitumor activity in rhabdomyosarcoma preclinical models. *Int J Cancer* 2007; **120**: 1141–9.

35 Shi Z, Peng XX, Kim IW *et al*. Erlotinib (Tarceva, OSI-774) antagonizes ATP-binding cassette subfamily B member 1 and ATP-binding cassette subfamily G member 2-mediated drug resistance. *Cancer Res* 2007; **67**: 11012–20.

36 Brendel C, Scharenberg C, Dohse M *et al*. Imatinib mesylate and nilotinib (AMN107) exhibit high-affinity interaction with ABCG2 on primitive hematopoietic stem cells. *Leukemia* 2007; **21**: 1267–75.

37 Polli JW, Humphreys JE, Harmon KA *et al*. The role of efflux and uptake transporters in N-{3-chloro-4-[(3-fluorobenzyl)oxy]phenyl}-6-[5-({[2-(methylsulfonyl)ethyl]amino} methyl)-2-furyl]-4-quinazolinamine (GW572016, lapatinib) disposition and drug interactions. *Drug Metab Dispos* 2008; **36**: 695–701.

38 Shukla S, Robey RW, Bates SE, Ambudkar SV. Sunitinib. (Sutent, SU11248), a small-molecule receptor tyrosine kinase inhibitor, blocks function of the ABC transporters, P-glycoprotein (ABCB1) and ABCG2. *Drug Metab Dispos* 2008; **37**: 359–65.

39 Dai CL, Liang YJ, Wang YS *et al*. Sensitization of ABCG2-overexpressing cells to conventional chemotherapeutic agent by sunitinib was associated with inhibiting the function of ABCG2. *Cancer Lett* 2009; **279**: 74–83.

40 Imai Y, Nakane M, Kage K *et al*. C421A polymorphism in the human breast cancer resistance protein gene is associated with low expression of Q141K protein and low-level drug resistance. *Mol Cancer Ther* 2002; **1**: 611–6.

41 Sparreboom A, Gelderblom H, Marsh S *et al*. Diflomotecan pharmacokinetics in relation to ABCG2 421C>A genotype. *Clin Pharmacol Ther* 2004; **76**: 38–44.

42 Cusatis G, Gregorc V, Li J *et al*. Pharmacogenetics of ABCG2 and adverse reactions to gefitinib. *J Natl Cancer Inst* 2006; **98**: 1739–42.

43 Rudin CM, Liu W, Desai A *et al*. Pharmacogenomic and pharmacokinetic determinants of erlotinib toxicity. *J Clin Oncol* 2008; **26**: 1119–27.

44 Yoshioka S, Katayama K, Okawa C *et al*. The identification of two germ-line mutations in the human *breast cancer resistance protein* gene in the expression of a low/non-functional protein. *Pharm Res* 2007; **24**: 1108–17.

45 Kawahara H, Noguchi K, Katayama K, Mitsuhashi J, Sugimoto Y. Pharmacologicalinteraction with sunitinib is abolished by a germ-line mutation (1291T>C) of BCRP/ABCG2 gene. *Cancer Sci* 2010; DOI: 10.1111/j.1349-7006.2010.01539.x. [Epub ahead of print].

Supporting Information

Additional Supporting Information may be found in the online version of this article:

Fig. S1. Expression of mutant breast cancer resistance protein (BCRP) in transfectant clones. Breast cancer resistance protein (BCRP) expression in a mixed population of cells and in nine transfectant clones was examined. Western blot analysis was performed under non-reducing (−SH) conditions. In lane PA/WT-mix(0.5), 0.5 μg protein was loaded on SDS–PAGE. (a) PA/WT cells; (b) PA/C592S cells; (c) PA/C603S cells; (d) PA/C608S cells; (e) PA/C592S·C603S cells; (f) PA/C592S·C603S cells; (g) PA/C603S·C608S cells; (h) PA/C592S·C603S·C608S cells.

Fig. S2. Mitoxantrone accumulation in mutant breast cancer resistance protein (*BCRP*) transfectants. Cells (5×10^5 were) were incubated in the presence or absence of 1 μM mitoxantrone for 40 min at 37°C, and then washed and resuspended in ice-cold PBS. Fluorescence was determined by flow cytometry. (a) PA317 cells; (b) PA/WT-mix cells; (c) PA/C592S-cl.6 cells; (d) PA/C603S-cl.3 cells; (e) PA/C592S·C608S-cl.7; (f) PA/C592S·C603S·C608S-cl.7 cells.

Fig. S3. Mitoxantrone accumulation in breast cancer resistance protein (*BCRP*)-knocked down cells. The mitoxantrone accumulation assay was performed in siRNA-transfected cells. (a) PA317 cells transfected with control siRNA (top) or *BCRP* siRNA (bottom). (b) PA/WT-mix cells transfected with control siRNA (top) or *BCRP* siRNA (bottom). (c) PA/C592S·C603S·C608S-cl.7 cells transfected with control siRNA (top) or *BCRP* siRNA (bottom).

Fig. S4. Localization of breast cancer resistance protein (BCRP) protein in mutant *BCRP* transfectants. The cells were stained with anti-BCRP antibody BXP-21 following an Alexa Fluor 488 goat antimouse antibody (green). Nuclei were stained with DAPI (blue). PA317 cells were also stained with BXP-21 and DAPI as a negative control. Breast cancer resistance protein (BCRP) and nuclei were observed using confocal microscopy.

Fig. S5. Schematic depiction of disulfide bridge in wild-type and mutant breast cancer resistance proteins (BCRPs). The dimer/monomer were determined using western blot analyses under non-reducing conditions (Fig. 3).

Please note: Wiley-Blackwell are not responsible for the content or functionality of any supporting materials supplied by the authors. Any queries (other than missing material) should be directed to the corresponding author for the article.

In vivo expansion of MDR1-transduced cells accompanied by a post-transplantation chemotherapy regimen with mitomycin C and methotrexate

Junko Mitsuhashi[1]
Hiroyo Hosoyama[1]
Satomi Tsukahara[2]
Kazuhiro Katayama[1]
Kohji Noguchi[1]
Yoshinori Ito[2]
Kiyohiko Hatake[2]
Keisuke Aiba[3]
Shunji Takahashi[2]
Yoshikazu Sugimoto[1,2]*

[1]*Division of Chemotherapy, Faculty of Pharmacy, Keio University, Tokyo, Japan*

[2]*Cancer Chemotherapy Center, Japanese Foundation for Cancer Research, Tokyo, Japan*

[3]*Department of Human Cancer, Jikei University School of Medicine, Tokyo, Japan*

*Correspondence to:
Yoshikazu Sugimoto, Division of Chemotherapy, Faculty of Pharmacy, Keio University, 1-5-30 Shibakoen, Minato-ku, Tokyo 105-8512, Japan. E-mail: sugimoto-ys@pha.keio.ac.jp

Abstract

Background A recurrent breast cancer patient received high-dose chemotherapy, a transplant of *multidrug resistance 1* (*MDR1*)-transduced cells and four different protocols of post-transplantation chemotherapy. We report the analysis of *MDR1*-transduced cells in this patient.

Methods *MDR1* transgene levels in the peripheral blood mononuclear cells of the patient were evaluated by polymerase chain reaction (PCR). Retroviral integration sites of the *MDR1*-transduced cells were identified by linear amplification-mediated (LAM)-PCR.

Results Twelve days after transplantation, approximately 1% of the peripheral blood mononuclear cells were *MDR1* transgene-positive. The transgene levels decreased quickly, and were at low levels until day 504. A remarkable increase in *MDR1* transgene-positive cells was observed on day 532, during combination chemotherapy with mitomycin C and methotrexate. Using LAM-PCR, 31 *MDR1*-transduced clones were identified, and eight of these were long-life clones that survived for more than 500 days. Among the 31 clones, ten had a retroviral integration site near genes listed in the Retroviral Tagged Cancer Gene (RTCG) Database. Two long-life clones, N-30 and N-31, had retroviral integration sites within the *MDS1-EVI1* locus. Another two long-life clones had integration sites close to *PRDM16* or *CUEDC1*.

Conclusions These results suggest that *MDR1*-transduced cells were enriched *in vivo* by an *MDR1* substrate, mitomycin C. The possible activation of *EVI1* or other RTCGs by retroviral insertion may have affected the survival and persistence of a proportion of the transduced cells. Copyright © 2010 John Wiley & Sons, Ltd.

Keywords breast cancer; CD34; gene therapy; hematopoietic stem cell; P-glycoprotein; retrovirus

Introduction

The human *multidrug resistance 1* (*MDR1*) gene encodes the plasma membrane P-glycoprotein (P-gp; ABCB1), which extrudes various structurally unrelated natural antitumor agents in an ATP-dependent manner. Expression of the *MDR1* gene confers resistance to various antitumor agents such as